

Sensitivity Analysis in Poro-Elastic and Poro-Visco-Elastic Models with Respect to Boundary Data

H.T. Banks, K. Bekele-Maxwell, L. Bociu, M. Noorman
Center for Research in Scientific Computation
Department of Mathematics
North Carolina State University
Raleigh, NC 27695-8212
and
G. Guidoboni

Indiana University Purdue University Indianapolis
402 N. Blackford St, LD270
Indianapolis, IN 46202-3267

February 24, 2017

Abstract

In this article we consider poro-elastic and poro-visco-elastic models inspired by problems in medicine and biology [12], and we perform sensitivity analysis on the solutions of these fluid-solid mixtures problems with respect to the imposed boundary data, which are the main drivers of the system. Moreover, we compare the results obtained in the elastic case vs. visco-elastic case, as it is known that structural viscosity of biological tissues decreases with age and disease. Sensitivity analysis is the first step towards optimization and control problems associated with these models, which is our ultimate goal.

Keywords: Sensitivity, poro-elastic, poro-visco-elastic, biological tissues, complex-step method

AMS classification: 49K40, 49Q12, 74B20, 35Q92, 46N60, 62P10.

This is the author's manuscript of the article published in final edited form as:

Banks, H., Bekele-Maxwell, K., Bociu, L., Noorman, M., & Guidoboni, G. (2017). Sensitivity analysis in poro-elastic and poro-visco-elastic models with respect to boundary data. *Quarterly of Applied Mathematics*, 75(4), 697–735. <https://doi.org/10.1090/qam/1475>

1 Introduction

Poro-elasticity refers to fluid flow within a deformable porous medium. Poro-elastic models were inspired by problems in geophysics and petroleum engineering, including reservoir engineering, environmental engineering, and earthquake engineering [11, 10, 14, 22, 23, 25, 35, 47, 50, 60, 61, 28, 30, 33, 49]. Due to all these applications, porous media flows have attracted a lot of mathematical attention. The development of the mathematical theory for these models begins with the one-dimensional analysis of Terzaghi [57] in 1925. However, it is the work by Biot [11] in 1941 that set the mathematical foundation for the study of fluid-solid mixture problems. Nowadays there are many mathematical results in the literature regarding their well-posedness [62, 42, 51, 54, 15] and associated numerical simulations [19, 43, 44, 45].

In all the problems mentioned above, the poro-elastic structures are represented by soil and rocks. However, other examples of poro-elastic structures include biological tissues, such as cartilage, bone, and vascularized tissues. Therefore poro-elastic models are now more and more frequently applied to fluid flows through biological or bio-engineered tissues, with applications in bioengineering and medicine [17, 18, 20, 29, 32, 41, 48, 52, 56]. In many of these biological applications, boundary data play a crucial role [55, 59, 40, 58]. For example, in bioengineering, changes in the stress conditions can lead to tissues with very different biophysical properties. In ophthalmology, changes in the intraocular pressure (IOP) can alter the stress conditions within the ocular tissues, such as the lamina cribrosa in the optic nerve head, and increase their susceptibility to damage [17, 26]. This is very important, as it is believed that the biomechanics of the lamina cribrosa plays an important role in the development and progression of glaucoma, a group of eye diseases that leads to damage to the optic nerve head, and ultimately, irreversible vision loss.

In comparison to rocks and soil, biological tissues exhibit both elastic and visco-elastic behaviors, as they are composed of both elastin and collagen. With this motivation in mind, the authors of [12] provided a theoretical and numerical analysis of poro-elastic and poro-viscoelastic models, focusing on the role of visco-elasticity in the fluid-solid mixtures considered. The work in [12] extends the available results on existence of solutions for these PDE systems by considering the general, nonlinear coupling case (with permeability depending nonlinearly on dilation), with Dirichlet and Neumann boundary conditions for both solid and fluid components. Moreover, the regularity properties of the data and their effect on the solutions are tracked and compared between the elastic and viscoelastic cases, as it is known that viscoelastic properties of biological tissues often vary with age, health, and disease. Interestingly, the study in [12] identified the time regularity of the imposed boundary traction as a crucial factor that guarantees boundedness of the solutions, and showed that the system dynamics fundamentally change as viscoelastic effects vanish. These findings are particularly relevant in the case of the lamina cribrosa in the eye, as they suggest that the lack of visco-elasticity may increase the susceptibility of the tissue to localized damage (due to irregularity in the discharge velocity and peaks in the fluid energy) as boundary sources of traction (represented by the intraocular pressure, in this case) experience sudden changes in time. However, sudden changes in intraocular pressure are physiological (they occur even when we rub our eyes). Therefore, the hypothesis in [12] is that the physiological changes in intraocular pressure can induce pathological changes in the hemodynamics of the lamina cribrosa tissue if the viscoelasticity provided by the collagen fibers is not intact.

The present work was inspired by and will further extend the analysis presented in [12]. The

goal of our effort here is to perform sensitivity analysis on the solutions of the poro-elastic and poro-visco-elastic models introduced in [12] with respect to the imposed boundary data, and to compare the results obtained in the purely elastic case vs. visco-elastic case. We will work in the framework of the numerical test cases considered in [12] for validation purposes. These cases include two stationary examples, where the data and the permeability of the tissue are constant, and two dynamical examples, where the permeability depends nonlinearly on the dilation, and the data are functions of space and time. The latter cases are obviously more challenging. From the theoretical point of view, we assume differentiability (in Banach spaces) of states with respect to data. From the numerical point of view, we will work with directional derivatives and take advantage of spline approximations.

Ultimately, sensitivity analysis provides valuable insights about how robust the fluid-mechanical responses are with respect to the changes of parameters and data and also reveals which ones are most influential in the system and can effectively be used as controls. Therefore, our work is intended as a precursor to efforts on optimization and optimal control problems. Our ultimate goal is to develop and address relevant control and optimization problems for the poro-visco-elastic models in order to develop novel strategies to improve experimental and clinical approaches in bioengineering and medicine.

We conclude the introduction with the description of the PDE model associated with the fluid-solid mixture problem that we are considering.

1.1 PDE Model

Let $\Omega \subset \mathbb{R}^3$ be an open domain occupied by the fluid-solid mixture. Let \mathbf{x} be the position vector of each point in the body with respect to a Cartesian reference frame, and $V_f(\mathbf{x}, t)$ the volume occupied by the fluid component in every representative elementary volume $V(\mathbf{x}, t)$ in Ω at time t . Then the *porosity* ϕ and the *fluid content* ζ are defined as

$$\phi(\mathbf{x}, t) = \frac{V_f(\mathbf{x}, t)}{V(\mathbf{x}, t)} \quad \text{and} \quad \zeta(\mathbf{x}, t) = \phi(\mathbf{x}, t) - \phi_0(\mathbf{x}).$$

where ϕ_0 is the baseline value for porosity.

Under the assumptions of negligible inertia, small deformations and incompressible mixture components [3, 24, 31, 34, 46], the motion of the poro-visco-elastic material is governed by the following equations for the balance of mass (of the fluid component) and linear momentum (for the fluid-solid mixture):

$$\zeta_t + \nabla \cdot \mathbf{v} = S(\mathbf{x}, t) \quad \text{and} \quad \nabla \cdot \mathbf{T} + \mathbf{F} = \mathbf{0} \quad \text{in } \Omega \times (0, T) \quad (1)$$

where \mathbf{T} is the total stress tensor of the mixture, \mathbf{v} is the discharge velocity, \mathbf{F} is a body force per unit of volume and S is a net volumetric fluid production rate.

The balance equations are completed with the following constitutive equations:

1. *Total stress* incorporates elastic and viscoelastic stress contributions, and is defined as

$$\mathbf{T} = \mathbf{T}_e + \delta \mathbf{T}_v - p \mathbf{I} = [2\mu_e \epsilon(\mathbf{u}) + \lambda_e (\nabla \cdot \mathbf{u}) \mathbf{I}] + \delta [2\mu_v \epsilon(\mathbf{u}_t) + \lambda_v (\nabla \cdot \mathbf{u}_t) \mathbf{I}] - p \mathbf{I}, \quad (2)$$

where $\epsilon(\mathbf{u}) = (\nabla\mathbf{u} + \nabla\mathbf{u}^T)/2$ is the symmetric part of the gradient of the vector field \mathbf{u} , p is the Darcy fluid pressure, \mathbf{u} is the solid displacement, \mathbf{I} is the identity tensor, λ_e and μ_e are the Lamé elastic parameters, and λ_v and μ_v are the viscoelastic parameters.

The parameter $\delta \geq 0$ indicates the extent to which the model includes viscoelastic effects for the solid component, with $\delta = 0$ corresponding to the purely elastic case.

2. *Discharge velocity:*

$$\mathbf{v} = -\mathbf{K}\nabla p, \quad \text{with } \mathbf{K} = k\mathbf{I} \quad \text{and} \quad k = k_{ref}f_k(\phi), \quad (3)$$

where \mathbf{K} is the permeability tensor, and k_{ref} is a reference value for the permeability of the mixture. It is assumed that \mathbf{K} depends on the porosity and that is a multiple of the identity tensor. The particular form of the relationship between the permeability k and the porosity ϕ is represented by the function $f_k(\phi)$ and it depends on the geometrical architecture of the pores inside the matrix and the physical properties of the fluid. Many studies have considered k to be constant, leading to a linear coupling between the equations for linear momentum and mass balance. However, in many applications k is not constant. If fluid flows through spherical particles, then the Carman-Kozeny formula [27] is used, namely $f_k(\phi) = \frac{\phi^3}{(1-\phi)^2}$. On the other hand, if fluid flows inside cylindrical pores, then the quadratic formula [17] is more appropriate, namely $f_k(\phi) = \phi^2$.

The theoretical analysis in [12] was performed for a general nonlinear permeability k , without specifying a particular expression for it. The current investigation considers both constant and nonlinear (Carman-Kozeny) cases for the permeability.

3. *Fluid content:*

$$\zeta = \nabla \cdot \mathbf{u}, \quad \text{implying that } \phi = \phi_0 + \nabla \cdot \mathbf{u}. \quad (4)$$

Equation (4) is a particular instance of the more general expression $\zeta = c_0p + \alpha\nabla \cdot \mathbf{u}$ [11], where c_0 is the constrained specific storage coefficient and α is the Biot-Willis coefficient. Under the assumption of incompressibility for the fluid and solid components of the mixture, which is often the case in biological applications, $c_0 = 0$ and $\alpha = 1$ [21]. As a consequence, the permeability k reduces to be a function of $\nabla \cdot \mathbf{u}$ only (rather than a function of both p and $\nabla \cdot \mathbf{u}$). Thus, $k = k(\phi) = k(\phi(\nabla \cdot \mathbf{u}))$ will be abbreviated as $k = k(\nabla \cdot \mathbf{u})$.

Using the constitutive equations, the balance equations (1) can be rewritten as:

$$\nabla \cdot (\mathbf{T}_e + \delta\mathbf{T}_v - p\mathbf{I}) = -\mathbf{F} \quad \text{and} \quad \nabla \cdot \mathbf{u}_t - \nabla \cdot (k(\nabla \cdot \mathbf{u})\nabla p) = S \quad \text{in } \Omega \times (0, T). \quad (5)$$

Boundary conditions: Let $\partial\Omega = \Gamma_D \cup \Gamma_N$ be the boundary of Ω , with $\Gamma_D = \Gamma_{D,p} \cup \Gamma_{D,v}$ and $\overline{\Gamma_D} \cap \overline{\Gamma_N}$ possibly nonempty. The subscripts N and D indicate conditions imposed on stress and displacement, respectively, whereas the subscript p and \mathbf{v} indicate conditions imposed on Darcy pressure and discharge velocity, respectively. The following boundary conditions are considered:

$$\mathbf{T}\mathbf{n} = \mathbf{g}, \quad \mathbf{v} \cdot \mathbf{n} = 0 \quad \text{on } \Gamma_N, \quad (6)$$

$$\mathbf{u} = \mathbf{0}, \quad p = 0 \quad \text{on } \Gamma_{D,p}, \quad (7)$$

$$\mathbf{u} = \mathbf{0}, \quad \mathbf{v} \cdot \mathbf{n} = \psi \quad \text{on } \Gamma_{D,v}. \quad (8)$$

Here, \mathbf{n} is the outward unit normal vector, and \mathbf{g} and ψ are given functions of space and time.

Initial conditions: In order to specify the initial conditions, it is useful to distinguish between the viscoelastic case, i.e., $\delta > 0$, and the purely elastic case, i.e., $\delta = 0$.

If $\delta > 0$, then we assume $\mathbf{u}(x, 0) = \mathbf{u}^0$ in Ω . If $\delta = 0$, we assume $\nabla \cdot \mathbf{u}(x, 0) = d_0$ in Ω , with d_0 for which there exist a \mathbf{u}^0 such that $\nabla \cdot \mathbf{u}^0 = d_0$.

The remainder of this paper is organized as follows. In Section 2, we describe the goals of this article, and briefly summarize the numerical method that we are using. In Section 3, we describe the recent results obtained in [12] on well-posedness and regularity of solutions for the fluid-solid mixture considered, which will be used subsequently. In Section 4, we introduce the simplification of the coupled system to the one-dimensional case, which is used for the numerical simulations. In Section 5, we present all our numerical results, including constant and nonlinear permeability and constant and dynamical data. Lastly, Section 6 is devoted to conclusions and future work.

2 Sensitivity Analysis

The main goal of this paper is to compute the sensitivity matrix $\frac{\partial(\mathbf{u}, p, \mathbf{v})}{\partial \mathbf{g}}$, as efficiently and accurately as possible. In general, there are various ways of approximating sensitivity derivatives. The most common ones (see [7, 8, 9] and the references therein) are analytic methods, finite difference approximation, automatic differentiation and the use of sensitivity equations. Analytic methods require the derivation and development of a program that is specific to each problem, hence inefficient. The finite difference method, while relatively easy and efficient to implement, suffers from cancellation error. Sensitivity equations are accurate and computationally inexpensive in the case of reasonably small systems. However, in our case, we are dealing with a nonlinear fluid-solid mixture, and the sensitivity system will result in a coupled system of linear equations for the sensitivities, coupled to the original nonlinear system. The numerical investigation of this new coupled system will be challenging and not very efficient.

More recently, the *complex-step* method has been used to calculate sensitivities [38, 39]. For a summary of the method, please see [4] and [5]. In short, approximating an analytic function f by its Taylor series expansion with a complex step ih provides the following *complex-step* derivative approximation $\frac{\partial f}{\partial x} \approx \frac{\text{Im}[f(x + ih)]}{h}$, for small step size parameter h (up to machine precision). The idea of using complex variables to estimate derivatives originated in [37, 36], and has become quite popular in aerodynamic optimization [1, 2, 38, 39, 53]. The complex-step estimate is suitable for use in numerical computing and is very accurate and extremely robust, while retaining a reasonable computational cost. We recently demonstrated the efficacy of use of the complex-step method for computing sensitivities for biological models in [4, 5]. The method is applied to examples of various complexity - ranging from time delayed differential equations (DDEs) (whose sensitivities are known to lack smoothness or even have discontinuities with respect to parameters such as the delays) to Lamé systems (where the boundary data-to-state map may not possess smoothness) - and the results are compared with solutions of traditional sensitivity equations. We observed that (i) the method is easy to implement, as no derivation of sensitivity equations is required, (ii) the complexity of the algorithm is the same as the complexity of the algorithm evaluating the solution function (i.e., the algorithm solving the system of equations), (iii) less computation time is needed if the number of parameters is not large compared to the dimension

of the problem, and (iv) the method gives consistently second order accurate approximation of the derivative starting from h as large as 10^{-2} down to $h_{crit} = 10^{-300}$ (approximately the machine zero at $h = 10^{-324}$) with a true second order accuracy. Moreover, we showed that, even though the complex-step formula is derived assuming analyticity of the solution function, the approximation provides accurate one-sided derivatives for functions with far less smoothness, implying that analyticity of the solution functions is sufficient but not necessary for the complex-step method to be effective.

2.1 Goals and Approaches

Using insight from our recent results in [4, 5], we compute the desired sensitivities using the complex-step derivative approach mentioned above, in combination with the dual mixed hybridized (DMH) finite element discretization developed for the nonlinear coupling in [12]. First, we apply the method to four one-dimensional test cases discussed in [12], for which analytical solutions are available. We use the first test case (where the data and the permeability are constants) to validate our technique. In the other three cases, while the analytic solutions are provided in [12] (either for $\delta = 0$ or $\delta = 1$), there is no explicit dependence on the boundary data in the formulas. So there is no analytic information about how sensitive the solution is to the given data. This is exactly the first scope of this current paper. Lastly, we perform sensitivity analysis on a one-dimensional, dynamical case with irregular (in time) boundary data. In this case, the numerical results in [12] predicted a finite time blow up for the fluid energy when the viscoelasticity is not present in the system. Our goal in this case is to compute and compare the sensitivities of the states with respect to the boundary data for $\delta = 0$ and $\delta = 1$, as well as treat δ as a control parameter, and see how the sensitivities change while δ takes a variety of values in two important ranges: $\delta < 1$ and $\delta \geq 1$.

3 Existence of Solutions and Regularity of Data

We include a summary of notation and existence of solutions results from [12], which are used in the present work. As the presence of visco-elasticity heavily influences the behavior of the solutions, the notions of solution and data are different depending on whether the parameter δ is strictly positive or is equal to zero. Using the following notation for the solution spaces and inner products

$$V \equiv H_{\Gamma_{D,p}}^1, \quad \mathbf{V} \equiv (H_{\Gamma_D}^1(\Omega))^3, \quad \mathbb{V} \equiv V \times \mathbf{V}, \quad (\cdot, \cdot) = (\cdot, \cdot)_{L^2(\Omega)}, \quad \langle \cdot, \cdot \rangle_{\Gamma} = \langle \cdot, \cdot \rangle_{L^2(\Gamma)}$$

and for the elastic bilinear form $a(\mathbf{u}, \mathbf{w}) = (\nabla \cdot \mathbf{u}, \nabla \cdot \mathbf{w}) + (\nabla \mathbf{u}, \nabla \mathbf{w}) + (\nabla \mathbf{u}, (\nabla \mathbf{w})^T)$, the weak solutions for $\delta > 0$ and $\delta = 0$ are defined as follows:

[Visco-Elastic Solution] $\mathbf{u} \in H^1(0, T; \mathbf{V})$ and $p \in L^2(0, T; V)$ such that for any $(q, \mathbf{w}) \in \mathbb{V}$ and $f \in C^\infty(0, T)$:

$$\begin{aligned} \delta \int_0^T a(\mathbf{u}_t, \mathbf{w}) f dt + \int_0^T a(\mathbf{u}, \mathbf{w}) f dt - \int_0^T (p, \nabla \cdot \mathbf{w}) f dt &= \int_0^T \langle \mathbf{g}, \mathbf{w} \rangle_{\Gamma_N} f dt - \int_0^T (\mathbf{F}, \mathbf{w}) f dt \\ \int_0^T (k(\nabla \cdot \mathbf{u}) \nabla p, \nabla q) f dt + \int_0^T (\nabla \cdot \mathbf{u}_t, q) f dt &= - \int_0^T \langle \psi, q \rangle_{\Gamma_{D,\nu}} f dt + \int_0^T (S, p) f dt \end{aligned}$$

with initial conditions $\mathbf{u}(\mathbf{x}, 0) = \mathbf{u}^0 \in \mathbf{V}$ and $\nabla \cdot \mathbf{u}(\mathbf{x}, 0) = d_0 \in L^2(\Omega)$ are given, and it is required that $\nabla \cdot \mathbf{u}^0 = d_0$ (in the $L^2(\Omega)$ sense).

[*Elastic Solution*] $\mathbf{u} \in L^2(0, T; \mathbf{V})$ and $p \in L^2(0, T; V)$ such that for any $(q, \mathbf{w}) \in \mathbb{V}$ and $f \in C_0^\infty(0, T)$:

$$\begin{aligned} \int_0^T a(\mathbf{u}, \mathbf{w}) f \, dt - \int_0^T (p, \nabla \cdot \mathbf{w}) f \, dt &= \int_0^T \langle \mathbf{g}, \mathbf{w} \rangle_{\Gamma_N} f \, dt - \int_0^T (\mathbf{F}, \mathbf{w}) f \, dt \\ \int_0^T (k(\nabla \cdot \mathbf{u}) \nabla p, \nabla q) f \, dt - \int_0^T (\nabla \cdot \mathbf{u}, q) f' \, dt &= - \int_0^T \langle \psi, q \rangle_{\Gamma_{D,\nu}} f \, dt + \int_0^T (S, p) f \, dt \end{aligned}$$

where for every $q \in V$, $(\nabla \cdot \mathbf{u}(t), q)$ uniquely defines an absolutely continuous function on $[0, T]$ and the initial condition $(\nabla \cdot \mathbf{u}(0), q) = (d_0, q)$ is satisfied.

When $\delta > 0$, the notion of *time differentiability* for the solution is stronger than in the case $\delta = 0$. As a consequence, time regularity requirements of the data are significantly weaker in the case $\delta > 0$ than in the case $\delta = 0$:

$$\begin{aligned} \text{DATA}_0 \Big|_0^T &\equiv \int_0^T \left[\|\mathbf{g}(t)\|_{L^2(\Gamma_N)}^2 + \|\psi(t)\|_{L^2(\Gamma_{D,\nu})}^2 + \|S(t)\|_{L^2(\Omega)}^2 + \|\mathbf{F}(t)\|_{L^2(\Omega)}^2 \right. \\ &\quad \left. + \|\mathbf{g}_t(t)\|_{L^2(\Gamma_N)}^2 + \|\mathbf{F}_t(t)\|_{L^2(\Omega)}^2 \right] dt + \sup_{[0,T]} \left[\|\mathbf{F}(t)\|^2 + \|\mathbf{g}(t)\|_{L^2(\Gamma_N)}^2 \right] \\ \text{DATA}_\delta \Big|_0^T &\equiv \int_0^T \left[\|\mathbf{g}(t)\|_{L^2(\Gamma_N)}^2 + \|\psi(t)\|_{L^2(\Gamma_{D,\nu})}^2 + \|S(t)\|_{L^2(\Omega)}^2 + \|\mathbf{F}(t)\|_{L^2(\Omega)}^2 \right] dt \end{aligned}$$

The following result on existence of solutions for the system (1)-(8) was obtained in [12]:

(a) If the data have the following regularity $\mathbf{F} \in L^2(0, T; (L^2(\Omega))^3)$, $S \in L^2(0, T; L^2(\Omega))$, $\mathbf{g} \in L^2(0, T; (H^{1/2}(\Gamma_N))^3)$, and $\psi \in L^2(0, T; L^2(\Gamma_{D,\nu}))$, then there exists a *visco-elastic solution* satisfying

$$\sup_{t \in [0, T]} E(\mathbf{u}(t)) + \int_0^T \left[E(p(t)) + E(\mathbf{u}(t)) + E(\mathbf{u}_t) \right] dt \leq C_1 \left[E(\mathbf{u}(0)) + \left(\frac{1}{1 + \delta} \right) \text{DATA}_\delta \Big|_0^T \right] e^{\frac{C_2 T}{1 + \delta}}.$$

(b) If data are of the form $\mathbf{F} \in H^1(0, T; (L^2(\Omega))^3)$, $S \in L^2(0, T; L^2(\Omega))$, $\mathbf{g} \in H^1(0, T; (H^{1/2}(\Gamma_N))^3)$, and $\psi \in L^2(0, T; L^2(\Gamma_{D,\nu}))$, then there exists an *elastic solution* satisfying

$$\sup_{t \in [0, T]} E(\mathbf{u}(t)) + \int_0^T \left[E(p(t)) + E(\mathbf{u}(t)) \right] dt \leq C_1 \left[E(\mathbf{u}(0)) + \text{DATA}_0 \Big|_0^T \right] e^{C_2 T}$$

where the energies associated to \mathbf{u} and p are defined as:

$$E(\mathbf{u}(t)) \equiv \frac{1}{2} \left[\|\nabla \cdot \mathbf{u}(t)\|^2 + \|\nabla \mathbf{u}\|^2 + (\nabla \mathbf{u}, \nabla \mathbf{u}^T) \right], \text{ and } E(p(t)) = (k(\nabla \cdot \mathbf{u}) \nabla p, \nabla p).$$

Note that purely elastic solutions require more time regularity for the volumetric source of linear momentum \mathbf{F} and the boundary traction source \mathbf{g} . The energy estimates predicted by the analysis were confirmed by numerical experiments for the 1D case when the data were sufficiently regular

[12]. In the purely elastic case, when the boundary traction datum did not enjoy sufficient time regularity for the estimates to hold (i.e., \mathbf{g} is only L^2 in time), the numerical experiments actually provided clues of energy blow-up, since (i) peaks appeared in the energy E_p in correspondence to the time discontinuity of the data (see Figure 1 below), (ii) the peaks got higher as the time discretization parameter tended to zero, and (iii) the behaviors of fluid pressure and discharge velocity were much less smooth in the purely elastic case than in the viscoelastic case.

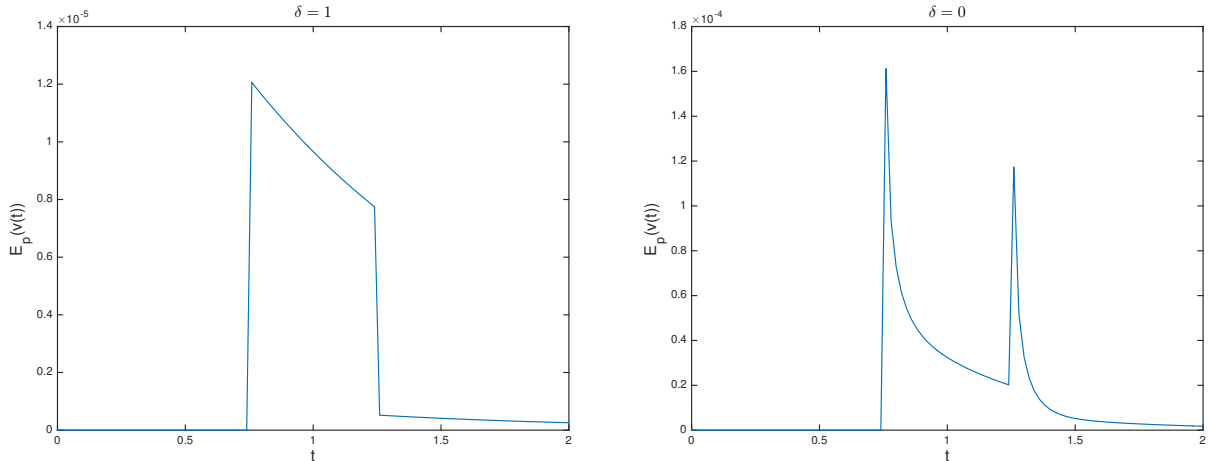


Figure 1: Computed energy E_p when the system is driven by the sole time irregular boundary source of traction

4 The 1D Poro-Visco-Elastic Model

For the numerical simulations, we follow [12] and focus on the 1D-counterpart model, with permeability either constant or nonlinearly dependent on dilation, following the Carman-Kozeny formula. We consider the computational domain $\Omega = (x_0, x_f)$ of length $L = x_f - x_0$ with boundary $\partial\Omega = \{x_0, x_f\}$ and outward unit normal vector n such that $n(x_0) = -1$ and $n(x_f) = +1$. We also define the computational time domain $t \in (t_0, t_f)$ of length $T = t_f - t_0$. The balance laws become

$$\frac{\partial \sigma}{\partial x} = -F \quad \text{and} \quad \frac{\partial \xi}{\partial t} + \frac{\partial v}{\partial x} = S. \quad (9)$$

The associated constitutive equations are given by

$$\sigma = 2\mu_e \frac{\partial u}{\partial x} - \wp + \delta \frac{\partial}{\partial t} \left[2\mu_v \frac{\partial u}{\partial x} - \frac{\lambda_v}{\lambda_e} \wp \right] - p, \quad (10)$$

$$\frac{\wp}{\lambda_e} + \frac{\partial u}{\partial x} = 0, \quad (11)$$

$$\xi = \frac{-\wp}{\lambda_e}, \quad (12)$$

$$v = -k \left(-\frac{\wp}{\lambda_e} \right) \frac{\partial p}{\partial x}, \quad (13)$$

and we have the following initial and boundary conditions:

$$u(x, t_0) = u_0(x) \quad \forall x \in \Omega, \quad (14)$$

$$\sigma(x, t)n(x, t) = g(x, t), \quad v(x, t)n(x, t) = 0 \quad \forall x \in \Gamma_N, \quad \forall t \in (t_0, t_f), \quad (15)$$

$$u(x, t) = 0, \quad p(x, t) = 0 \quad \forall x \in \Gamma_{D,p}, \quad \forall t \in (t_0, t_f), \quad (16)$$

$$u(x, t) = 0, \quad v(x, t)n(x) = \psi(x) \quad \forall x \in \Gamma_{D,v}, \quad \forall t \in (t_0, t_f). \quad (17)$$

In terms of notation, we use σ as the one-dimensional analogue of the stress tensor \mathbf{T} defined in (2). Note that $\Gamma_N \cup \Gamma_{D,p} \cup \Gamma_{D,v} = \partial\Omega = \{x_0, x_f\}$, and that $\Gamma_N, \Gamma_{D,p}$ and $\Gamma_{D,v}$ can be empty (but not all of them simultaneously). We would like to point out that the introduction of the elastic pressure parameter \wp in this one-dimensional version avoids displacement differentiation in the evaluation of the permeability and prevents from degradation of computational accuracy (see [12] for more details on this issue). We do not need to impose any boundary conditions for \wp , since the total stress is already prescribed on Γ_N in (15).

The 1D counterparts of the 3D-expressions for the energies are given by

$$\begin{aligned} E_e(u(t)) &= \frac{1}{2}(\lambda_e + 4\mu_e) \left\| \frac{\partial u(x, t)}{\partial x} \right\|_{L^2(\Omega)}^2 & \forall t \in (t_0, t_f), \\ E_v(u(t)) &= \frac{1}{2}(\lambda_v + 4\mu_v) \left\| \frac{\partial u(x, t)}{\partial x} \right\|_{L^2(\Omega)}^2 & \forall t \in (t_0, t_f), \\ E_p(p(t)) &= \left\| \sqrt{k \left(-\frac{\wp}{\lambda_e} \right)} \frac{\partial p(x, t)}{\partial x} \right\|_{L^2(\Omega)}^2 = \left\| \frac{1}{\sqrt{k \left(\frac{-\wp}{\lambda_e} \right)}} v(x, t) \right\|_{L^2(\Omega)}^2 & \forall t \in (t_0, t_f). \end{aligned}$$

In the numerical results, we consider the sensitivity of solution (u, p) with respect to g in both elastic and visco-elastic cases. We will also compute the sensitivity of the discharge velocity v with respect to g , as the numerical simulations in [12] hint at blow up in the fluid energy E_p in the case of non-smooth boundary traction g and no visco-elasticity ($\delta = 0$) present in the system.

5 Main Results

In this section we present our numerical examples. We perform sensitivity analysis on the one-dimensional poro-visco-elastic model described in Section 2.2 with respect to the boundary source of traction g , following the same test cases considered in [12]. For the discretization in space, we use the numerical approach based on DMH finite elements [12]. Moreover, we use the Backward Euler (BE) method to advance in time (both procedures are documented in detail in [12]). For computing sensitivity functions, the complex-step method is built into the DMH algorithm and implemented as follows:

Step 1: Define all functions and operators that are not defined for complex arguments such as for example *max*, *min* and *abs* in the program used. For this work, we use MATLAB programming language, hence we redefine the Matlab functions appropriately.

Step 2: Add a small complex step ih to the desired sensitivity parameter ' x ', and run the DHM/BE solver to obtain $U(\cdot, x + ih)$.

Step 3: Compute $\partial U/\partial x$ using the formula $\frac{\partial U}{\partial x} \approx \frac{\text{Im}[U(\cdot, x + ih)]}{h}$. For all of our computations we take $h = 10^{-40}$.

First we validate our procedure, by considering a simple case where the data and the permeability are constants, and therefore the problem reduces to a stationary case, for which we have an analytic solution.

5.1 Constant Data, Constant Permeability - Case 1 (Validation)

Let the domain be given by $\Omega = (0, 1)$ of length $L = 1$. Consider the purely elastic ($\delta = 0$) system (9)-(17) in Ω , with constant volumetric sources F_1 and S_1 , constant boundary data g_1 and ψ_1 , and boundary conditions given by

$$\begin{cases} u = p = 0, & x_0 = 0, \\ \sigma n = g_1 \text{ and } v n = \psi_1, & x_f = 1. \end{cases} \quad (18)$$

This problem admits the following analytic solution, provided in [12]:

$$\begin{aligned} u(x) &= \frac{x}{H_A} \left[F_1 \left(L - \frac{x}{2} \right) + g_1 \right] - \frac{x^2}{2H_A k_{\text{ref}}} \left[\psi_1 - S_1 \left(L - \frac{x}{3} \right) \right], \\ p(x) &= \frac{x}{H_A} \left[S_1 \left(L - \frac{x}{2} \right) - \psi_1 \right], \\ \varphi(x) &= -\frac{\lambda_e}{H_A} (\sigma(x) + p(x)), \\ \sigma(x) &= g_1 + F_1(L - x), \\ v(x) &= \psi_1 + S_1(x - L), \end{aligned}$$

with $H_A = \lambda_e + 2\mu_e = 3$. If we treat the boundary data as parameters and thus assume that $g_1, \psi_1 \in \mathbb{R}$, and we consider the following specific values for the reference value of the permeability and the Lamé constants

$$k = k_{\text{ref}} = 1 \text{ cm}^3 \text{sg}^{-1}, \lambda_e = \mu_e = 1 \text{ dyne cm}^{-2}, \phi = 0.5,$$

we can simplify the formulas for the the solutions to

$$\begin{aligned} u(x, g_1, \psi_1) &= -\frac{S_1}{18} x^3 - \frac{1}{6} (F_1 + \psi_1 - S_1) x^2 + \frac{1}{3} (F_1 + g_1) x, \\ p(x, g_1, \psi_1) &= -\frac{S_1}{2} x^2 + (S_1 - \psi_1) x, \\ \sigma(x, g_1, \psi_1) &= g_1 + F_1(1 - x), \\ v(x, g_1, \psi_1) &= \psi_1 + S_1(x - 1). \end{aligned}$$

and find the partial derivatives with respect to g_1 and ψ_1 :

$$\frac{\partial u}{\partial g_1} = \frac{x}{3}, \quad \frac{\partial p}{\partial g_1} = 0, \quad \text{and} \quad \frac{\partial v}{\partial g_1} = 0. \quad (19)$$

For the numerical computations, we assume that the volumetric and boundary source terms are given by the following specific values:

$$F_1 = 0.3 \text{ dyne cm}^{-3}, \quad S_1 = 0.3 \text{ s}^{-1}, \quad g_1 = -0.3 \text{ dyne cm}^{-2}, \quad \psi_1 = -3 \text{ cm s}^{-1}.$$

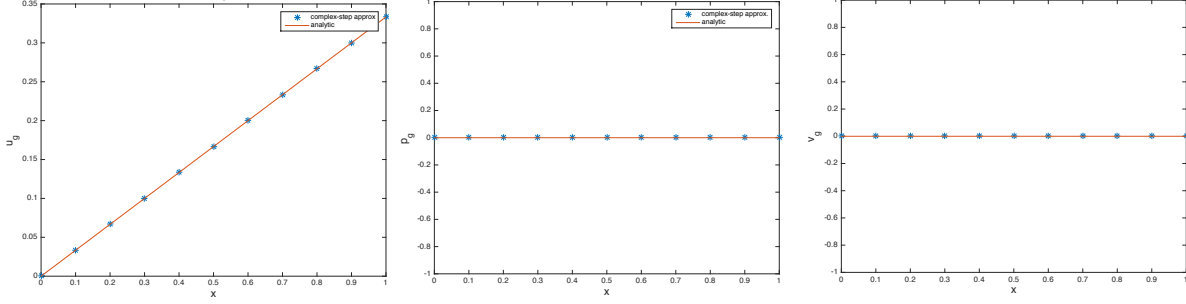


Figure 2: Sensitivity functions u , p and v with respect to g_1 at $g_1 = .3$

The computed sensitivities $\frac{\partial(U,v)}{\partial g_1}$ at $g_1 = 0.3$ [with $U = (u, p)$] are shown in Figure 2.

Observations: From Figure 2, we can see that the sensitivity derivatives obtained via the complex-step method agree with the ones computed analytically (19). We would also like to point out that the sensitivity of the elastic displacement to the boundary source g_1 at $g_1 = .3$ increases in magnitude as we approach the right end point $x_f = 1$ at which the boundary conditions are applied, which is to be expected.

5.2 Constant Boundary Data, Variable Permeability - Case 2

Let $\Omega = (-1, 1)$ of length $L = 2$. Consider the fluid-solid mixture (9)-(17) with $\delta = 0$, and homogeneous Dirichlet boundary conditions at $x_0 = -1$ and non-homogenous Neumann boundary conditions at $x_f = 1$:

$$\begin{cases} u = p = 0, & x_0 = -1, \\ \sigma n = g_2, \quad v n = \psi_2, & x_f = 1. \end{cases} \quad (20)$$

Volumetric and boundary source terms are given by:

$$\begin{aligned} F_2(x) &= -[U_{\text{ref}} H_A \chi''(x) - P_{\text{ref}} \chi'(x)], \\ S_2(x) &= -k_{\text{ref}} P_{\text{ref}} \chi''(x) \Theta(x) - k_{\text{ref}} P_{\text{ref}} U_{\text{ref}} \chi'(x) \chi''(x) \Xi(x), \\ \psi_2 &= -k_{\text{ref}} P_{\text{ref}} \chi'(x_f) \Theta(x_f), \end{aligned}$$

where

$$\begin{cases} \chi(x) = \sin(\omega_x x), & \Phi(x) = \phi_0 + U_{\text{ref}} \chi'(x), & \Theta(x) = \frac{\Phi^3(x)}{[1-\Phi(x)]^2}, & \Xi(x) = \frac{\Phi^2(x)[3-\Phi(x)]}{[1-\Phi(x)]^3}, \\ \omega_x = 2\pi/L, & U_{\text{ref}} = 0.1 \text{ cm}, & P_{\text{ref}} = 1 \text{ dynecm}^{-2}, & H_A = 3 \text{ dynecm}^{-2}, & \phi_0 = 0.5. \end{cases}$$

In comparison to the previous case, the porosity ϕ is now allowed to vary with the derivative of the displacement within the range $[\Phi_{\min}, \Phi_{\max}]$, where $0 < \Phi_{\min} < \Phi_{\max} < 1$, in such a way that the permeability k , expressed by the nonlinear relation of Carman-Kozeny, satisfies the following lower and upper bounds [16]

$$0 < k_{\text{ref}} \frac{\Phi_{\min}^3}{(1 - \Phi_{\min}^2)^2} \leq k(\phi) \leq k_{\text{ref}} \frac{\Phi_{\max}^3}{(1 - \Phi_{\max}^2)^2}.$$

Here we set $\Phi_{\min} = 0.125$, $\Phi_{\max} = 0.875$ and $k_{\text{ref}} = 1 \text{ cm}^3 \text{ s g}^{-1}$.

Due to the particular choice of data and implicitly, the structure of the solutions, we can see that the discharge velocity does not depend on g_2 , therefore v_2 is not sensitive to g_2 . However, elastic displacement u and fluid pressure p depend nonlinearly and implicitly on g_2 .

Similarly to Case 1, we consider g_2 as a constant parameter and compute the sensitivities of the states with respect to g_2 at $g_2 = -0.9425$. The numerical results agree with the analytical ones in the case of the discharge velocity. For u and p , we don't have explicit dependence on the boundary data.

Observations: We can see in Figure 3 that in comparison to Case 1, the peaks in sensitivity for both u and p are in the interior of the domain, which could be explained by the nonlinearity of the permeability, but also by the fact that the volumetric source of momentum is also non-zero and thus the solution is not driven solely by the boundary traction.

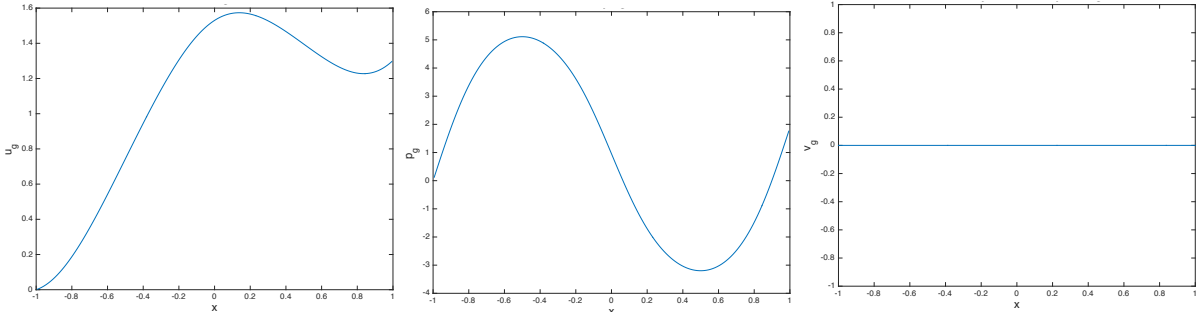


Figure 3: Sensitivity functions of u , p and v with respect to g_2

5.3 Dynamical Poro-Visco-Elastic Model, Constant Permeability - Case 3

In this example, we consider the problem (9)-(17) on $(0, L) \times (t_0, t_f) = (0, 1) \times (0, .1)$, with boundary conditions given by $u = p = 0$ at $x_0 = 0$, and $\sigma n = g_3(t)$ and $vn = \psi_3(t)$ at $x_f = 1$. We prescribe the following volumetric and boundary source terms

$$\begin{aligned} F_3(x, t) &= -U_{\text{ref}}\chi''(x)[H_A\tau(t) + \delta H_V\tau'(t)] - P_{\text{ref}}\tau(t)\chi'(x), \\ S_3(x, t) &= U_{\text{ref}}\tau'(t)\chi'(x) - k_{\text{ref}}P_{\text{ref}}\chi''(x)\tau(t), \\ \psi_3(t) &= -k_{\text{ref}}P_{\text{ref}}\tau(t)\chi'(x_f), \end{aligned}$$

where the spatial and temporal shape functions are given by

$$\begin{cases} \chi(x) = \sin(\omega_x x), & \text{with } \omega_x = 8/L \\ \tau(t) = \sin^2(\omega_t t), & \text{with } \omega_t = 8/t_f, \end{cases}$$

respectively, and the parameters have the following values: $U_{\text{ref}} = 0.1$ cm, $P_{\text{ref}} = 0.3$ dyne cm⁻², $H_A = \lambda_e + 2\mu_e = 3$ dyne cm⁻², and $H_V = \lambda_v + 2\mu_v = 0.5774$ dyne s cm⁻².

As in Case 1, we assume that the porosity and permeability are constant and given by $\phi = \phi_0 = 0.5$ and $k = k_{\text{ref}} = 1$ cm³sg⁻¹, respectively.

The boundary source g_3 is now a function of time. Therefore, assuming that the data-to-state map is Gâteaux differentiable, we compute the directional derivatives of the state (u, p) and v with

respect to the function g_3 in an arbitrary direction \bar{g} . We approximate both the data and the directions using linear splines. We partition the time interval $[0, .1]$ into ten subintervals of equal length $\Delta t = .01$. We define $\phi_i : [-.01, 0.11] \rightarrow \mathbb{R}$ for $i = 1, \dots, 11$ as follows:

$$\phi_i(t) = \begin{cases} \frac{t-t_{i-1}}{\Delta t}, & \text{for } t \in [t_{i-1}, t_i] \\ \frac{t_{i+1}-t}{\Delta t}, & \text{for } t \in [t_i, t_{i+1}] \\ 0, & \text{otherwise,} \end{cases}$$

with the understanding that $t_1 = 0$ and $t_{11} = .1$. We use these eleven splines to approximate g_3 ,

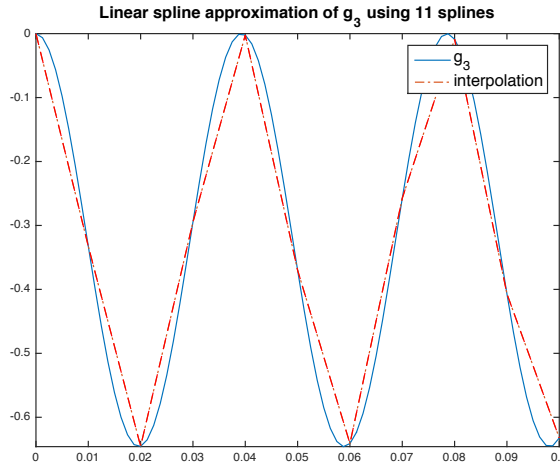


Figure 4: Linear spline approximation of g_3

with $\alpha_i = g_3(t_i)$ (see Figure 4): $g_3(t) \approx g_{3h} = \sum_{i=1}^{11} \alpha_i \phi_i(t)$.

Moreover, we consider $\bar{g} \in \text{span}\{\phi_i\}_1^{11}$, and write it as $\bar{g}(t) = \sum_{i=1}^{11} \bar{\alpha}_i \phi_i(t)$.

By the chain rule, we have that $D_\alpha u = (D_{g_{3h}} u)(D_\alpha g)$. Note that $(D_\alpha g_{3h})[\bar{\alpha}_1 \quad \bar{\alpha}_2 \quad \dots \quad \bar{\alpha}_{11}]^T = \bar{g}$. Therefore

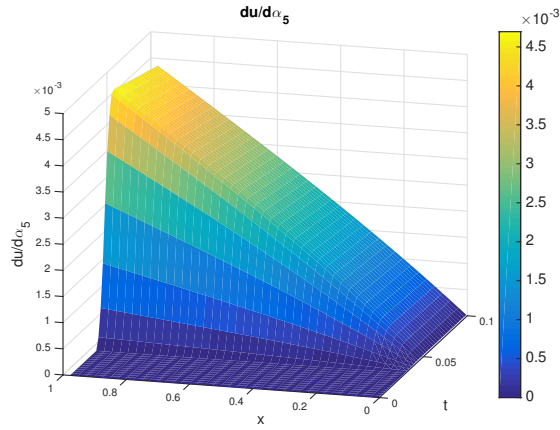
$$(D_{g_{3h}} u)\bar{g} = (D_\alpha u)[\bar{\alpha}_1 \quad \bar{\alpha}_2 \quad \dots \quad \bar{\alpha}_{11}]^T,$$

which means that the action of the directional derivative of u with respect to g_{3h} is completely defined through the vector $D_\alpha u$, and the structure of the direction [13]. Thus it is sufficient to numerically compute the derivatives of the states with respect to the parameters α_i , which represent the values of g_3 at specific times t_i .

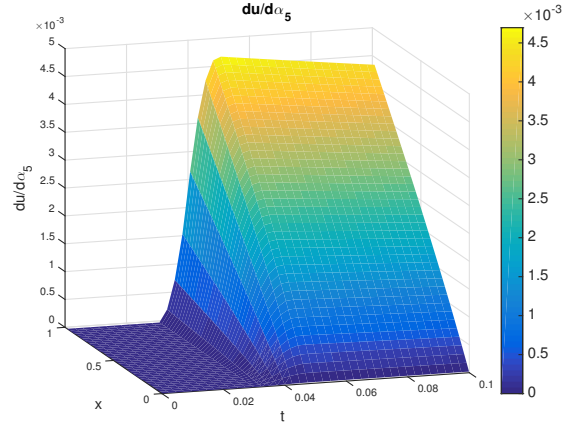
In the figures below, we display the graphs of the directional derivatives first in the case of directions taken as particular splines, like ϕ_1 and ϕ_2 , and then for specific linear combinations of the splines, like $\bar{g} = \sum_{i=1}^{11} \phi_i$. For all the sensitivities, we include both visco-elastic and purely elastic cases, and compare the results.

Sensitivity graphs with respect to boundary source g_3

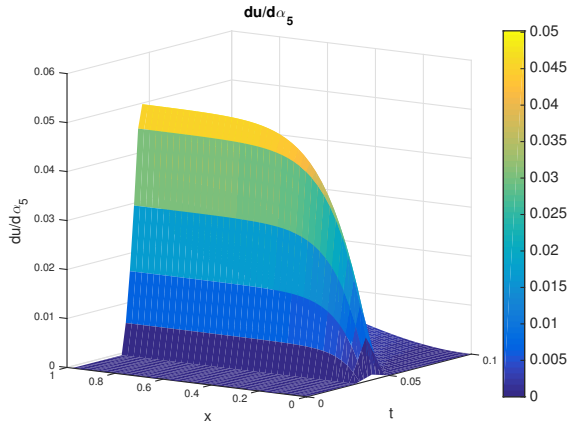
$$1. (D_{g_{3h}} u)\phi_5 = \frac{\partial u}{\partial \alpha_5}$$



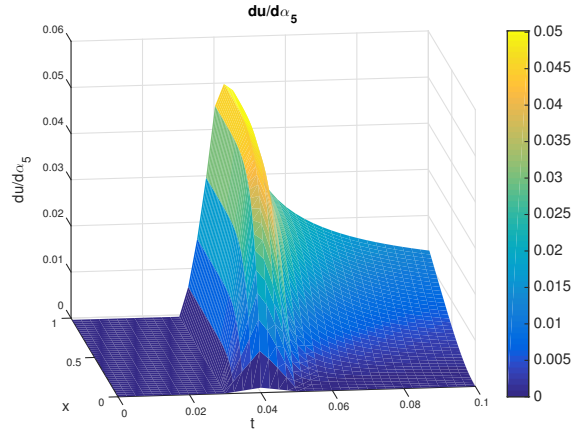
$\delta = 1$



$\delta = 1$ (different angle of view)



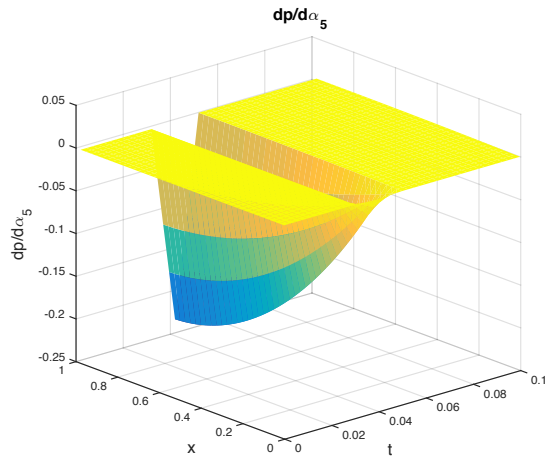
$\delta = 0$



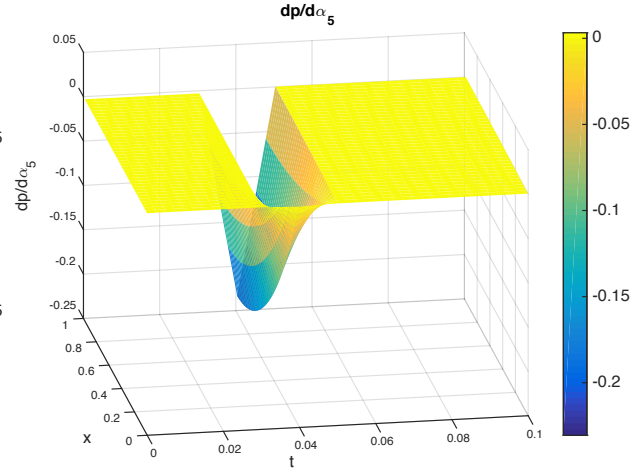
$\delta = 0$ (different angle of view)

Figure 5: Sensitivity functions of solid displacement u with respect to boundary stress g_{3h} in the direction of ϕ_5 , when $\delta = 1$ (top) and $\delta = 0$ (bottom).

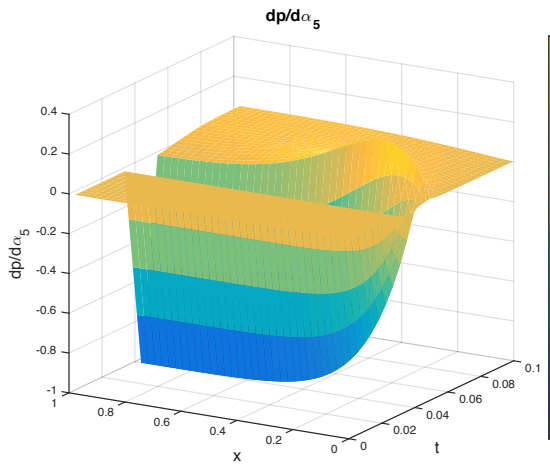
$$2. (D_{g_{3h}} p)\phi_5 = \frac{\partial p}{\partial \alpha_5}$$



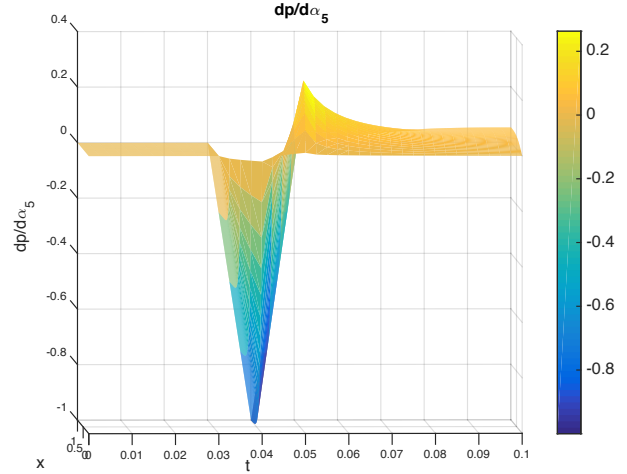
$\delta = 1$



$\delta = 1$ (different angle of view)



$\delta = 0$



$\delta = 0$ (different angle of view)

Figure 6: Sensitivity functions of fluid pressure p with respect to boundary stress g_{3h} in the direction of ϕ_5 when $\delta = 1$ (top) and $\delta = 0$ (bottom).

$$3. (D_{g_{3h}} v)\phi_i = \frac{\partial v}{\partial \alpha_i}, \quad i = 1, 4$$

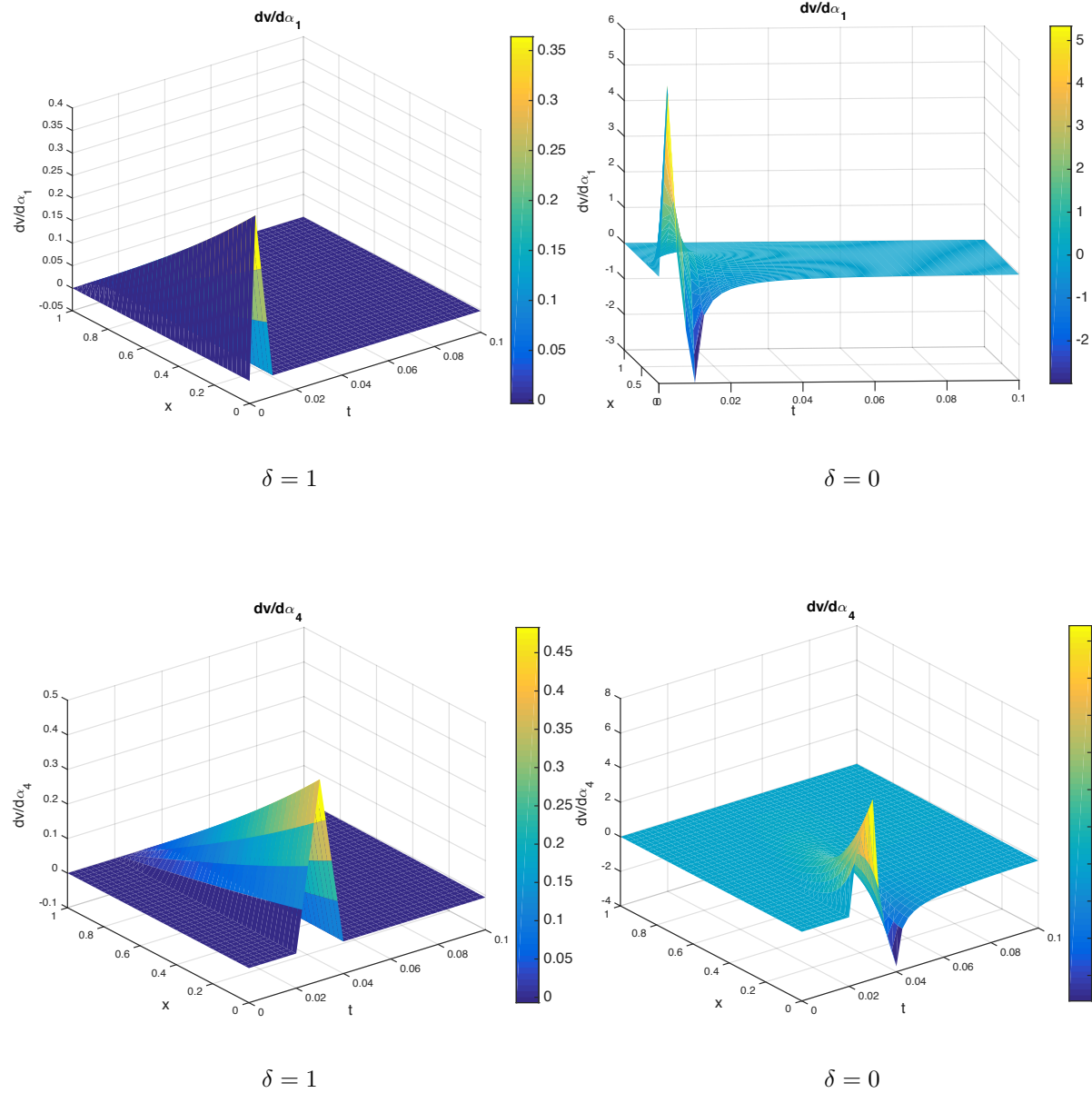
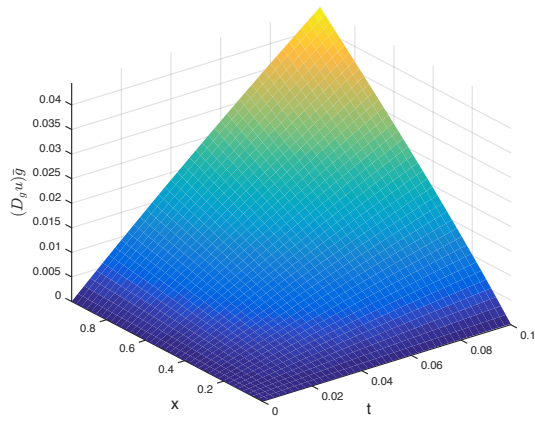
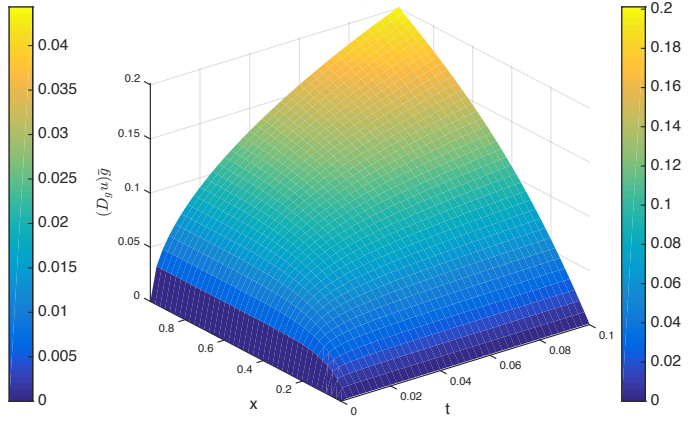


Figure 7: Sensitivity functions of discharge velocity (v) with respect to boundary stress g_{3h} in the direction of ϕ_i , $i = 1, 4$ for model test case 2 when $\delta = 1$ (left) and $\delta = 0$ (right).

$$4. (D_{g_{3h}} u) \bar{g}, \bar{g} = \sum_{i=1}^{11} \phi_i$$

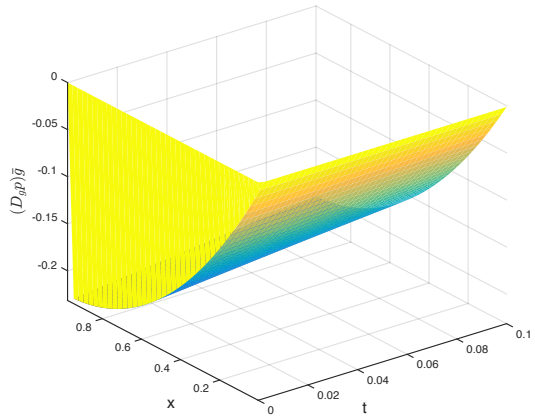


$\delta = 1$

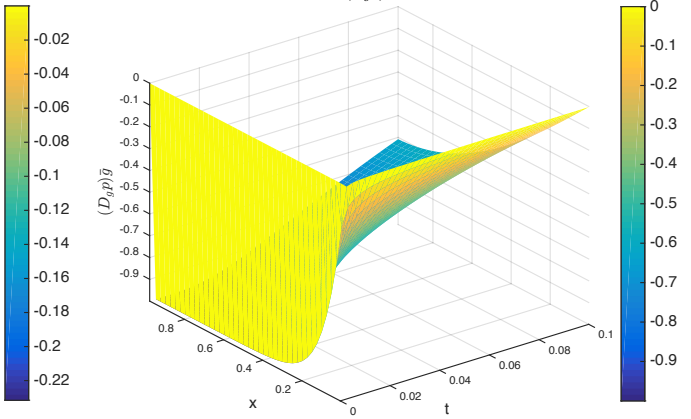


$\delta = 0$

$$5. (D_{g_{2h}} p) \bar{g}, \bar{g} = \sum_{i=1}^{11} \phi_i$$



$\delta = 1$



$\delta = 0$

Figure 8: Sensitivity functions of solid displacement u and fluid pressure p with respect to boundary stress g_{3h} in the direction of $\bar{g} = \sum_{i=1}^{11} \phi_i$ when $\delta = 1$ (left) and $\delta = 0$ (right).

6. $(D_{g_{3h}} v) \bar{g}, \bar{g} = \sum_{i=1}^{11} \phi_i$

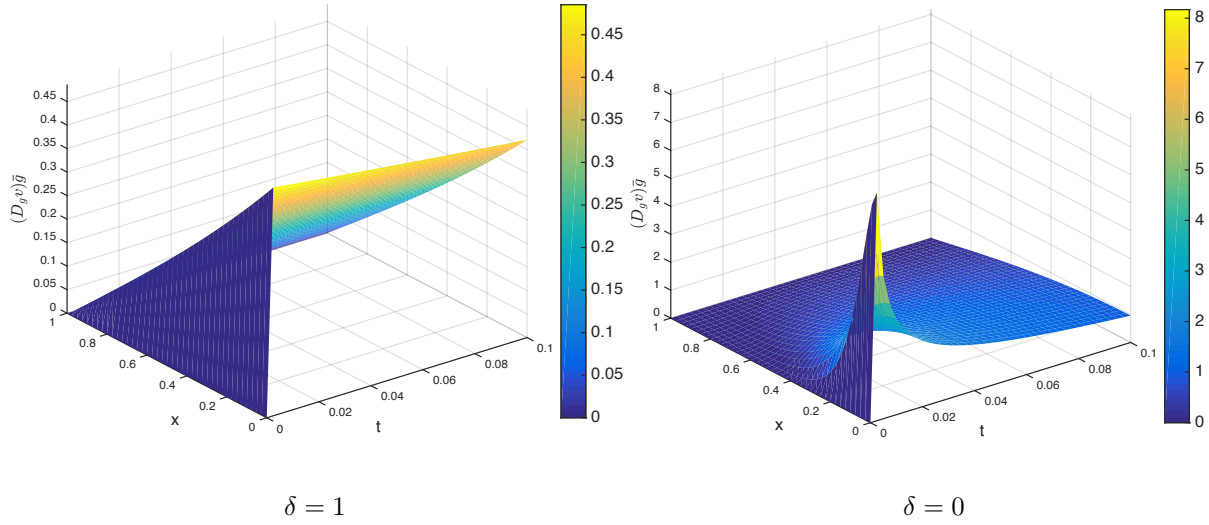


Figure 9: Sensitivity functions of discharge velocity v with respect to boundary stress g_{3h} in the direction of $\bar{g} = \sum_{i=1}^{11} \phi_i$ when $\delta = 1$ (left) and $\delta = 0$ (right).

Observations: From Figures 5-9 we can see that in the purely elastic case ($\delta = 0$), the sensitivities of all three states (u, p, v) are higher (by one order of magnitude) than in the visco-elastic case ($\delta = 1$).

Moreover, for $\delta = 1$, the sensitivity of u and p decreases as we go farther from the part of the boundary where the data g_{3h} is applied. In comparison, for $\delta = 0$, the solution is affected by the boundary datum g_{3h} throughout the entire domain. For $\delta = 1$, we see that the sensitivities $\frac{\partial u}{\partial \alpha_i}$ stay similar for $t \geq t_i$, whereas for $\delta = 0$, the sensitivities drops shortly after $t = t_i$. This could indicate the effect of the term $\frac{\partial u}{\partial t}$ in equation (9) is dominant in the case $\delta = 1$.

Comparing all the figures above, we can see that the discharge velocity v and the pressure p are the most sensitive to the boundary data g_{3h} . In the case of visco-elasticity, the magnitude of $\frac{\partial v}{\partial g_{3h}}$ is the highest among all of sensitivities. Moreover, the sensitivity is one order of magnitude higher in the case of $\delta = 0$, and two sharp peaks appear around the time at which the direction is given.

We also notice that in both elastic and visco-elastic cases, the sensitivity of the discharge velocity with respect to g , which is applied at $x = 1$, increases towards the left end point, $x = 0$, of the domain. This is due to the fact that at $x = 1$, $v \cdot n = \psi_3$ and ψ_3 is not dependent on g_3 . This results in $\frac{\partial v}{\partial g_3} \cdot n = 0$ at $x = 1$. The magnitude of $\frac{\partial v}{\partial g_3}$ increases as we go farther away from $x = 1$, and ultimately reaches its maximum at $x = 0$, as there is no condition imposed on v at this boundary point.

5.4 Dynamical Model with Variable Permeability - Case 4

Consider problem (9)-(17) in the space-time domain $(-1, 1) \times (0, T)$, so that $L = 2\text{cm}$ and $T = 2\text{s}$. The boundary conditions are given by

$$\begin{cases} u = p = 0, & x_0 = -1 \\ \sigma n = g_4(t), \quad vn = \psi_4(t), & x_f = 1. \end{cases}$$

Porosity and permeability are nonlinear functions of the solution, just as in Case 2. The volumetric and boundary source terms are time-dependent and are given by:

$$\begin{aligned} F_4(x, t) &= -[U_{ref}\chi''(x)(H_A\tau(t) + \delta H_V\tau'(t)) - P_{ref}\tau(t)\chi'(x)], \\ S_4(x, t) &= U_{ref}\chi'(x)\tau'(t) - P_{ref}k_{ref}\chi''(x)\tau(t)\Theta(x, t) - k_{ref}P_{ref}U_{ref}\chi'(x)\chi''(x)\tau^2(t)\Xi(x, t), \\ \psi_4(t) &= -k_{ref}P_{ref}\Theta(x_{end})\chi'(x_{end})\tau(t), \end{aligned}$$

where:

$$\begin{aligned} \chi(x) &= \sin(\omega_x x), \quad \tau(t) = \sin(\omega_t t), \quad \Phi(x, t) = \phi_0 + U_{ref}\chi'(x)\tau(t), \\ \Theta(x, t) &= \frac{\Phi^3(x, t)}{[1 - \Phi(x, t)]^2}, \quad \Xi(x, t) = \frac{\Phi^2(x, t)[3 - \Phi(x, t)]}{[1 - \Phi(x, t)]^3}, \end{aligned}$$

with $\omega_t = 2\pi/T$ and all the other parameter values given as in Case 3.

Again, since the boundary source g_4 is time dependent, we approximate this function using linear splines (described in Case 3):

$$g_4(t) \approx g_{4h} = \sum_{i=1}^{N_g} \alpha_i \phi_i(t), \quad \text{with } N_g = 11,$$

where $\alpha_i = g_4(t_i)$ (see Figure 10).

We computed the sensitivities with respect to all the parameters α_i , for $i = 1, \dots, 11$. These represent the directional derivatives of the solution with respect to boundary source in the directions of the splines ϕ_i . We display here two representative cases, i.e., for α_1 and α_4 . Then we consider the linear combination of splines $\bar{g} = \sum_{i=1}^{11} \phi_i$ as a specific direction and compute the associated sensitivities. All the results are displayed for both $\delta = 0$ and $\delta = 1$.

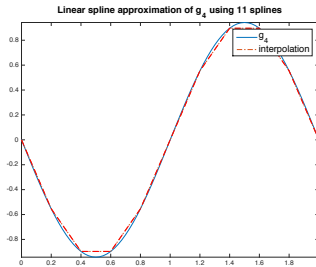


Figure 10: Linear spline approximation of g_4 .

Sensitivity graphs with respect to g_4

$$1. (D_{g_{4h}} u)\phi_i = \frac{\partial u}{\partial \alpha_i}, \quad i = 1, 4$$

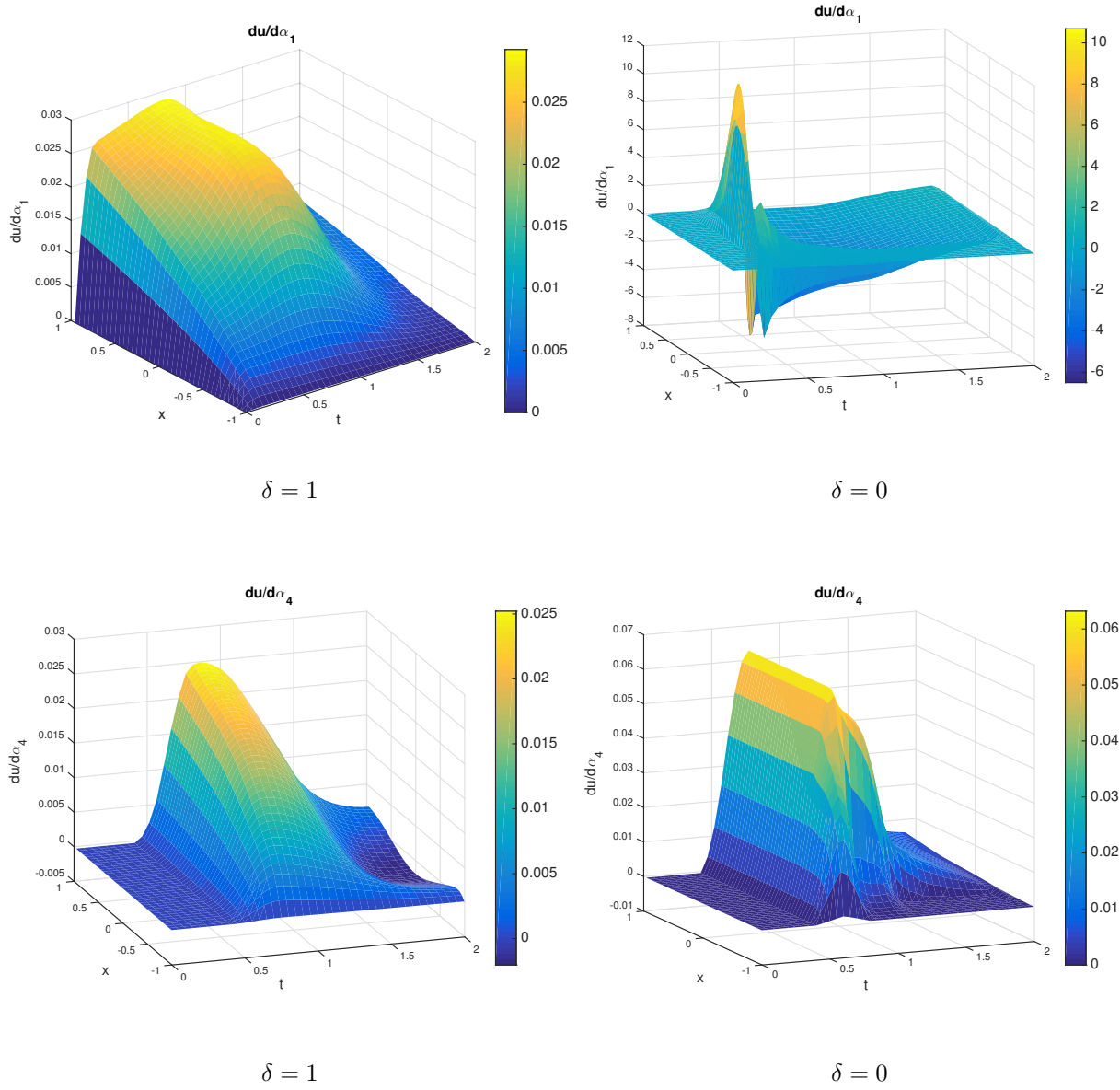
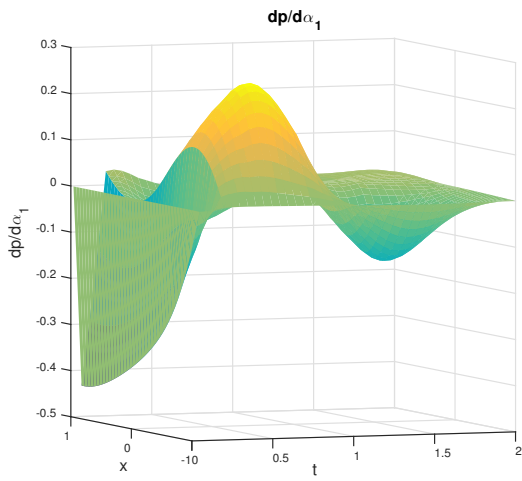
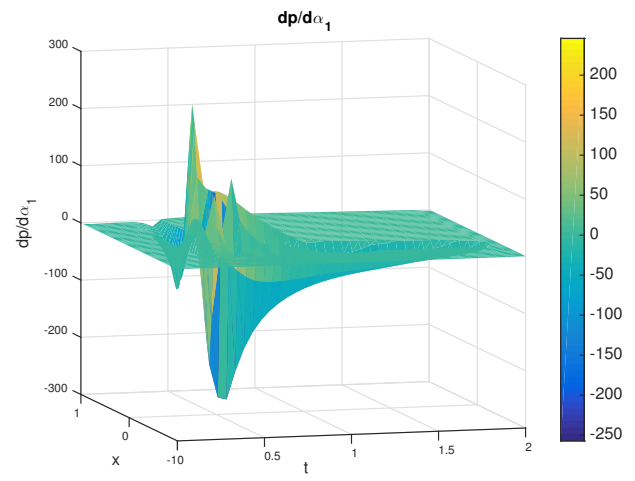


Figure 11: Sensitivity functions of solid displacement u with respect to boundary stress g_{4h} in the direction of ϕ_i , $i = 1, 4$ when $\delta = 1$ (left) and $\delta = 0$ (right).

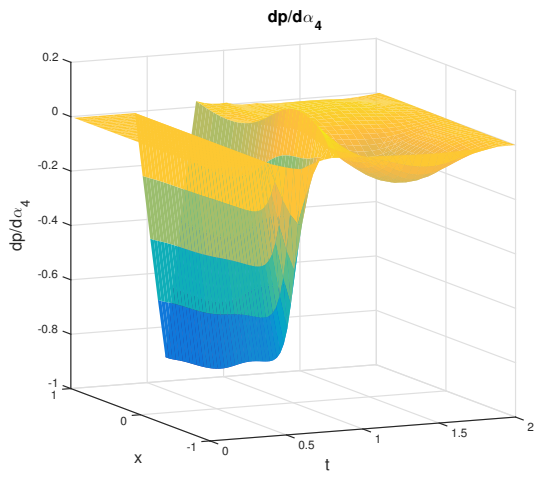
$$2. (D_{g_{4h}}p)\phi_i = \frac{\partial p}{\partial \alpha_i}, \quad i = 1, 4$$



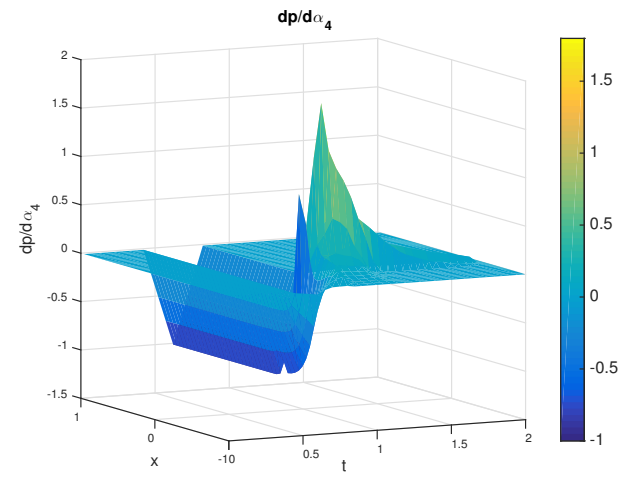
$\delta = 1$



$\delta = 0$



$\delta = 1$



$\delta = 0$

Figure 12: Sensitivity functions of pressure (p) with respect to boundary stress g_{4h} in the direction of ϕ_i , $i = 1, 4$ when $\delta = 1$ (left) and $\delta = 0$ (right).

$$3. (D_{g_{4h}} v)\phi_i = \frac{\partial v}{\partial \alpha_i}, \quad i = 1, 4$$

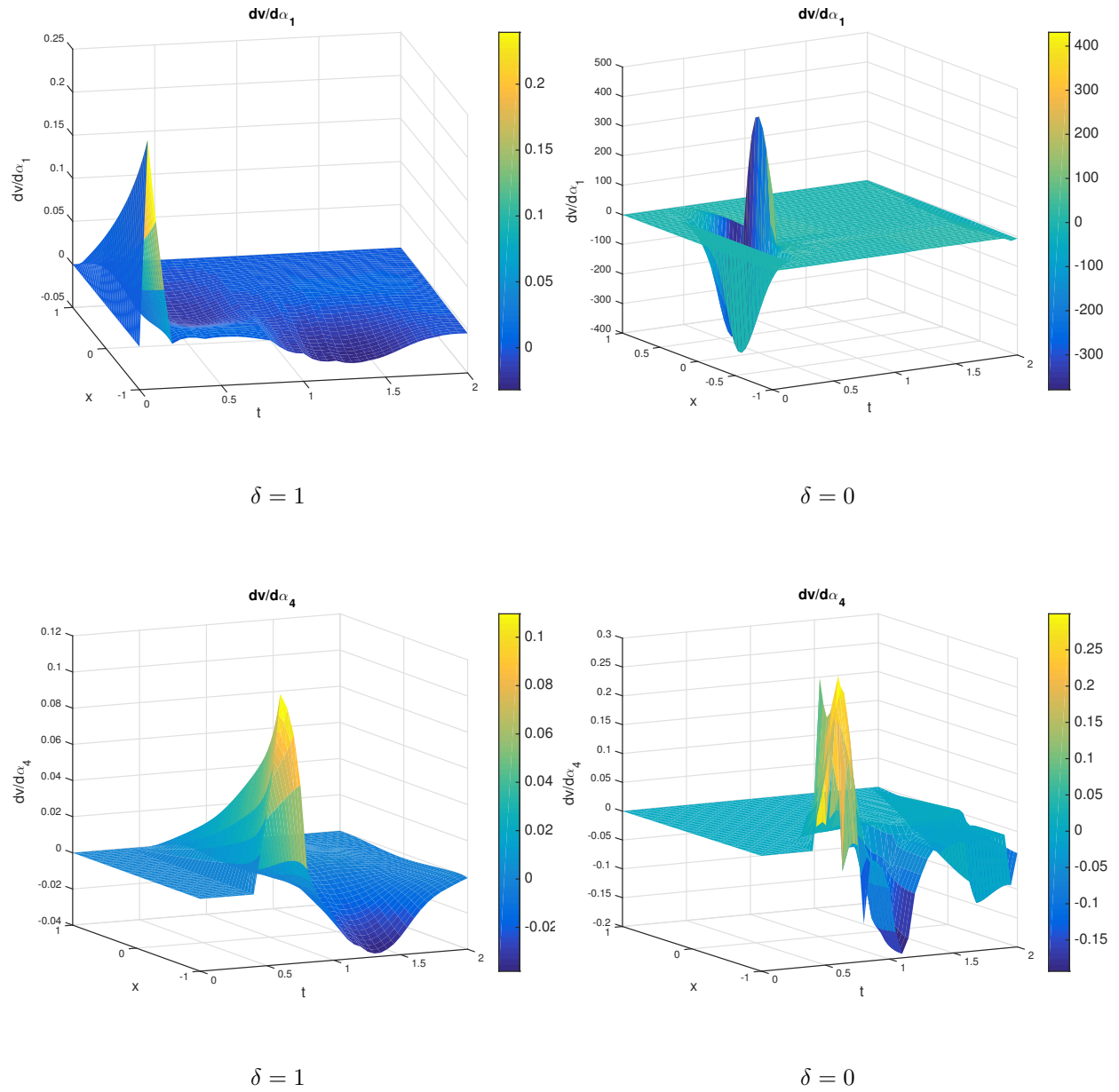
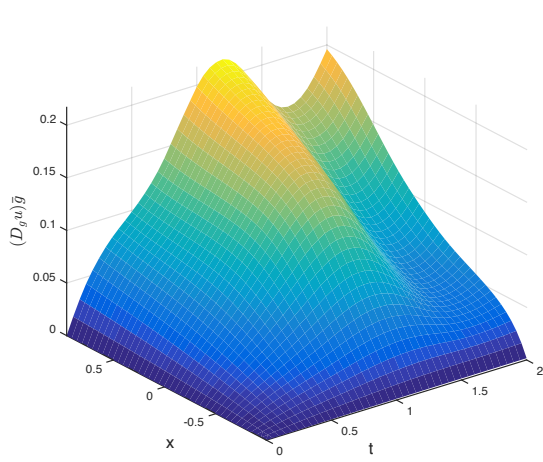
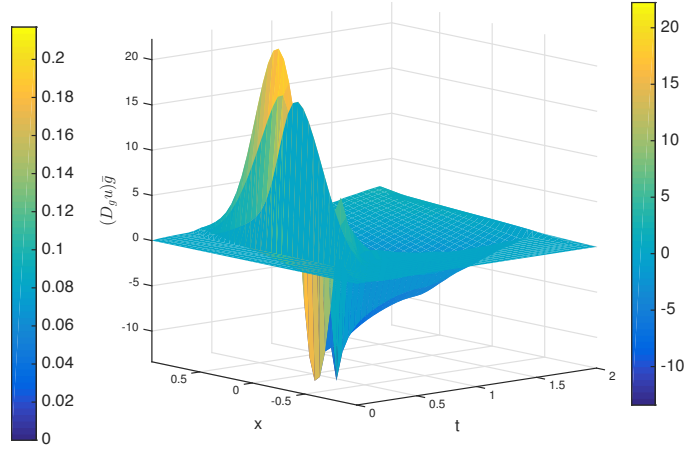


Figure 13: Sensitivity functions of discharge velocity v with respect to boundary stress g_{4h} in the direction of ϕ_i , $i = 1, 4$ when $\delta = 1$ (left) and $\delta = 0$ (right).

$$4. (D_{g_{Ah}} u) \bar{g}, \bar{g} = \sum_{i=1}^{11} \phi_i$$

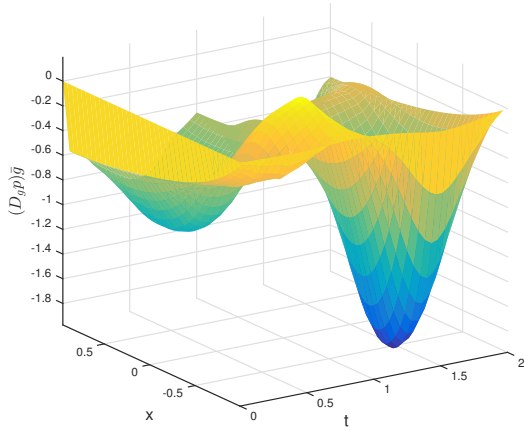


$\delta = 1$

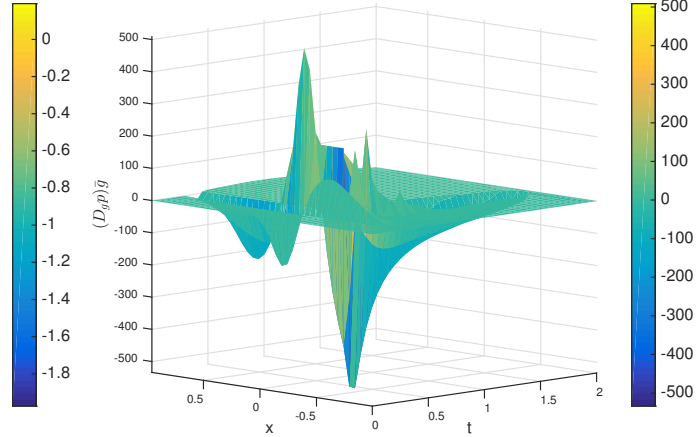


$\delta = 0$

$$5. (D_{g_{Ah}} p) \bar{g}, \bar{g} = \sum_{i=1}^{11} \phi_i$$



$\delta = 1$



$\delta = 0$

Figure 14: Sensitivity functions of solid displacement u and fluid pressure p with respect to boundary stress g_{Ah} in the direction of $\bar{g} = \sum_{i=1}^{11} \phi_i$ when $\delta = 1$ (left) and $\delta = 0$ (right).

6. $(D_{g_{Ah}} v) \bar{g}$, $\bar{g} = \sum_{i=1}^{11} \phi_i$

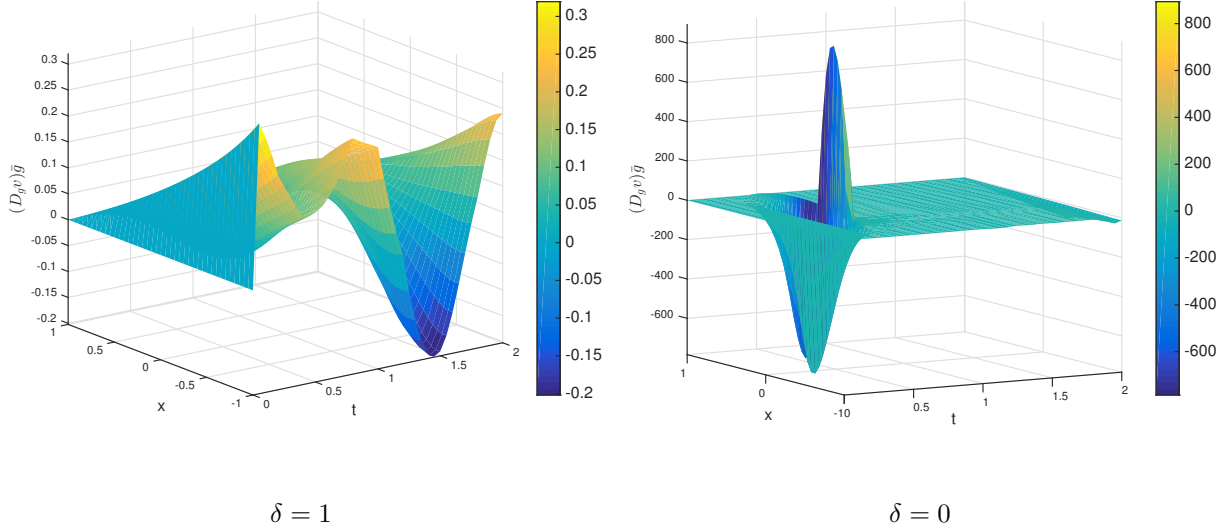


Figure 15: Sensitivity functions of discharge velocity v with respect to boundary stress g_{Ah} in the direction of $\bar{g} = \sum_{i=1}^{11} \phi_i$ when $\delta = 1$ (left) and $\delta = 0$ (right).

Observations: Regarding the elastic displacement u and pressure p , we can see from Figures 11, 12, 13 and 14, that the magnitude of the sensitivities is higher (up to 3 times in order of magnitude in the case of α_1) in the elastic case than in the visco-elastic case. The difference decreases for subsequent α_i 's.

Moreover, in the visco-elastic case, the sensitivity of u and p with respect to the boundary datum in the specific directions of the splines decreases as we get farther away from the boundary $x = 1$, where the datum acts. In comparison, the elastic displacement and pressure seem to be equally sensitive to the boundary source throughout the space domain in the purely elastic case. This is similar to Case 3, where the same behaviour was observed between the elastic and visco-elastic cases. However, this is not the case for the sensitivity in the direction \bar{g} , where the influence of the boundary is seen throughout the space-time domain. It can be observed though that in the visco-elastic case, the sensitivity surface is much smoother than in the elastic counterpart.

It is interesting to see the difference in behaviors of the sensitivities of the elastic displacement and pressure in comparison to Case 3, where the permeability is assumed to be constant. The surfaces associated with the sensitivities in this case are much more complex, with sharp peaks (present in the $\delta = 0$ scenario), and a non-zero presence almost throughout the space-time domain.

Some of the observations described above remain similar in the case of the discharge velocity v . In Figure 13, we can see that the magnitude of the sensitivity with respect to the particular spline directions ϕ_i 's are significantly bigger (ranging between 1 and 3 times in order of magnitude) in the case $\delta = 0$ vs. $\delta = 1$. Moreover, we can easily see that the discharge velocity, among the three state variables, is the most sensitive to the boundary datum. This could explain the fact

that the fluid energy (which is dependent on the discharge velocity and the permeability) seemed to become unbounded when the data loses smoothness in time [12].

We can also see that the surfaces associated with the velocity sensitivities in this case are less smooth and much sharper in this case than in Case 3 (where permeability is constant).

In comparison to the elasticity and pressure sensitivities, the sensitivity of the velocity with respect to the boundary data seems to increase towards the left end point $x = -1$ of the domain, in both the elastic and visco-elastic cases. This was explained when first observed in Case 3.

5.5 Irregular Boundary Data - Case 5

In [12], the following example is used to study how time regularity in the boundary source term influences the elastic stress and fluid pressure in the presence and absence of viscosity. Let us consider the problem (9)-(13) in the space-time domain $(-1, 1) \times (0, 2)$, so that $L = 2$ cm and $T = 2$ s. To help us see the effect better, we study the problem in the absence of volumetric sources of linear momentum and mass:

$$F_5(x, t) = S_5(x, t) = 0,$$

with the following initial and boundary conditions:

$$\begin{cases} u(x, t_0) &= 0, \quad \forall x \in \Omega, \\ u(x_0, t) &= p(x_0, t) = vn(x_f, t) = 0, \quad \forall t \in (t_0, t_f) \\ \sigma n(x_f, t) &= g_5 = \bar{g}\mathcal{G}_q(t; t_a, t_b) \quad \forall t \in (t_0, t_f), \end{cases}$$

where

$$\begin{cases} \mathcal{G}_q(t; t_a, t_b) = \frac{1}{2}[\tanh(q(t - t_a)) - \tanh(q(t - t_b))], & t_a = 1 - T/8, t_b = 1 + T/8, q = 100, \\ \bar{g} = 0.01 \text{ dynecm}^{-2}. \end{cases}$$

We approximate g_5 using the linear splines described in Case 3, namely, $g_5(t) \approx g_{5h} = \sum \alpha_i \phi_i$, $i = 1, \dots, 21$. As usual, the sensitivity functions are computed using the complex-step method. The results are shown in Figures 17 through 19.

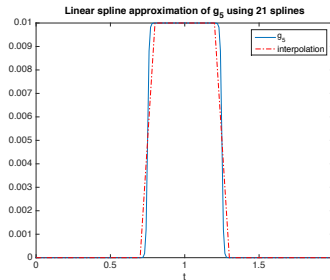


Figure 16: Linear spline approximation of g_5 .

Sensitivity graphs with respect to g_5

1. $(D_{g_{5h}} u)\phi_i = \frac{\partial u}{\partial \alpha_i}, i = 1, 6$

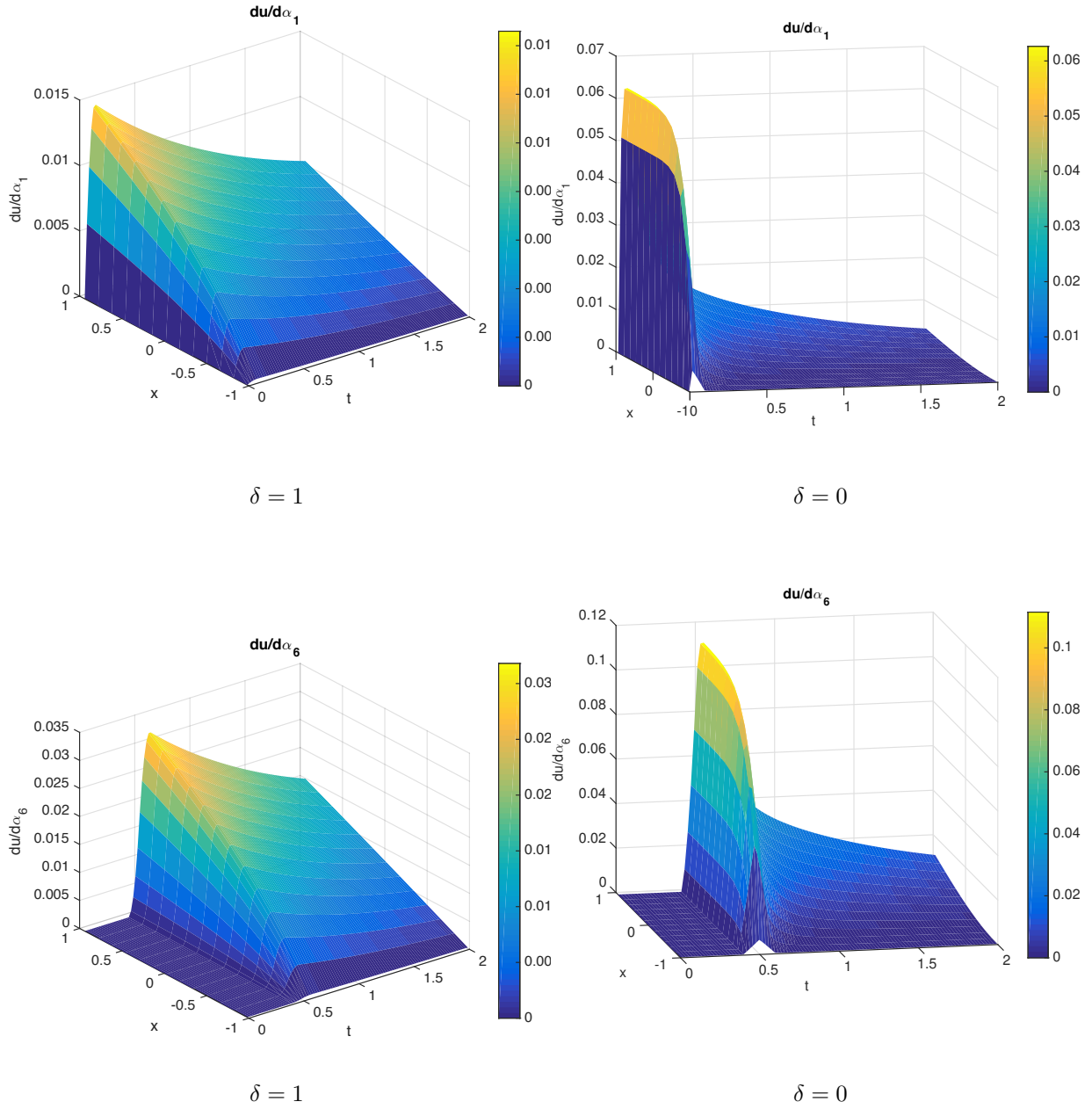


Figure 17: Sensitivity functions of solid displacement (u) with respect to boundary stress g_{5h} in the direction of ϕ_i , $i = 1, 6$ when $\delta = 1$ (left) and $\delta = 0$ (right).

$$2. (D_{g_{5h}}p)\phi_i = \frac{\partial p}{\partial \alpha_i}, \quad i = 1, 6$$

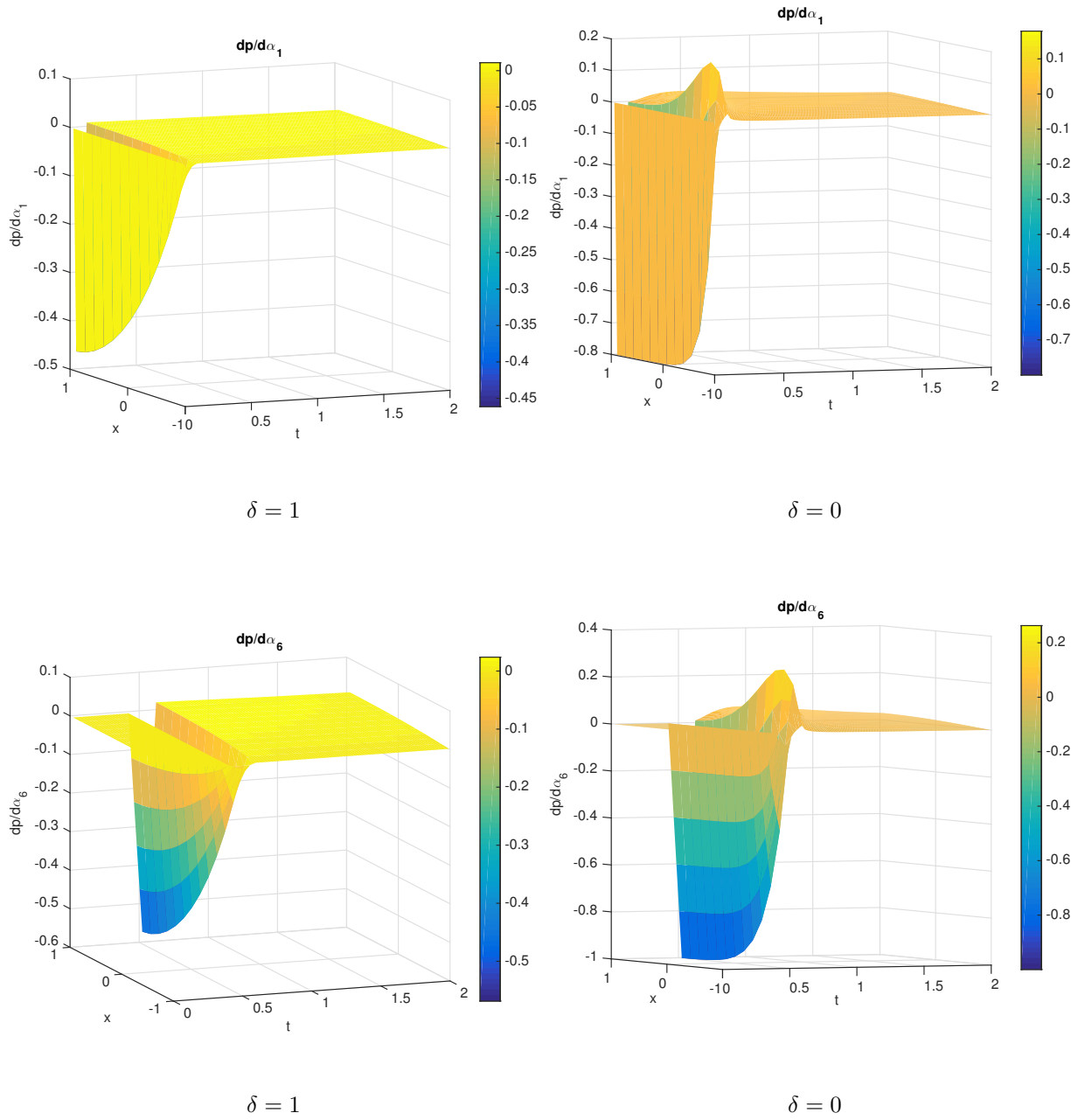


Figure 18: Sensitivity functions of pressure (p) with respect to boundary stress g_{5h} in the direction of ϕ_i , $i = 1, 6$ for model test case 5 when $\delta = 1$ (left) and $\delta = 0$ (right).

$$3. (D_{g_{5h}} v)\phi_i = \frac{\partial v}{\partial \alpha_i}, \quad i = 1, 6$$

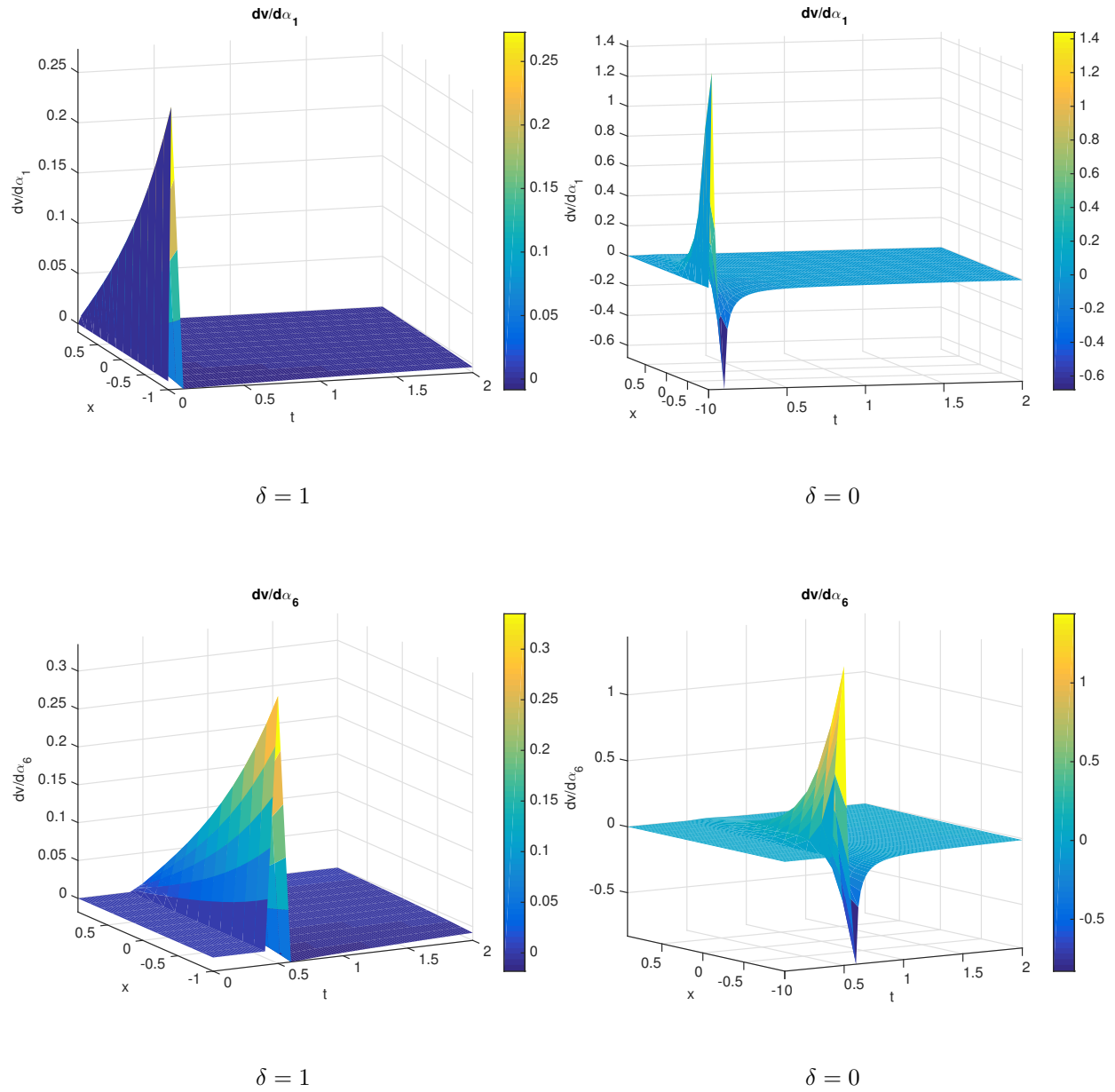
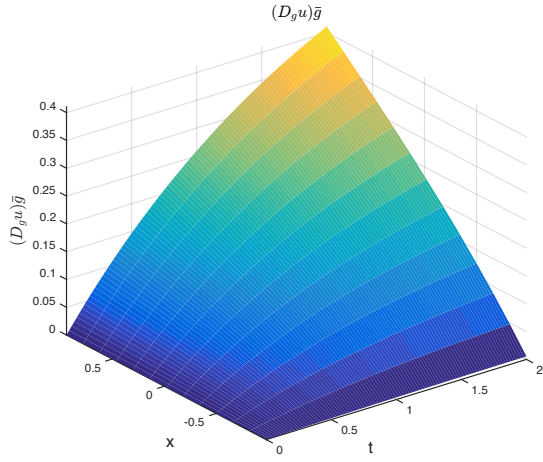
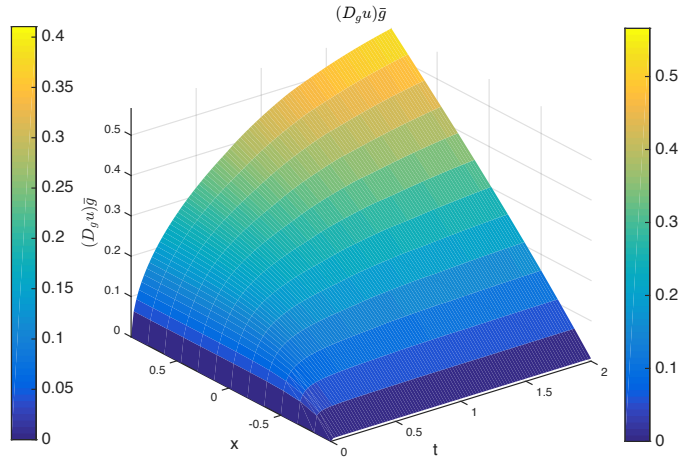


Figure 19: Sensitivity functions of discharge velocity (v) with respect to boundary stress g_{5h} in the direction of ϕ_i , $i = 1, 6$ when $\delta = 1$ (left) and $\delta = 0$ (right).

$$4. (D_{g_{5h}} u) \bar{g}, \bar{g} = \sum_{i=1}^{21} \phi_i$$

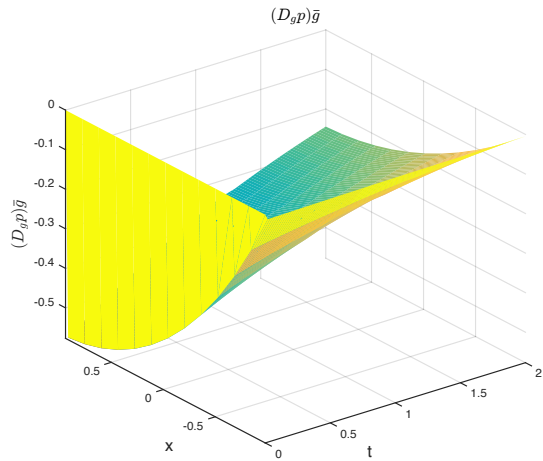


$\delta = 1$

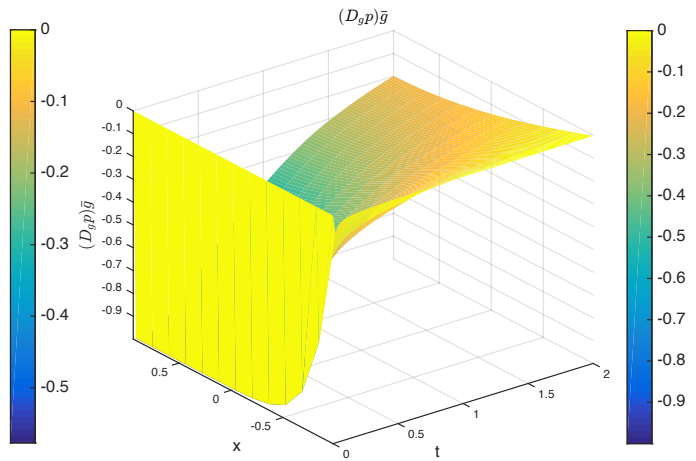


$\delta = 0$

$$5. (D_{g_{5h}} p) \bar{g}, \bar{g} = \sum_{i=1}^{21} \phi_i$$



(a) $\delta = 1$



(b) $\delta = 0$

Figure 21: Sensitivity functions of solid displacement u and fluid pressure p with respect to boundary stress $g_5 = \mathcal{G}_q, q = \infty$ in the direction of $\bar{g} = \sum_{i=1}^{21} \phi_i$ when $\delta = 1$ (left) and $\delta = 0$ (right).

$$6. (D_{g_5 h} v) \bar{g}, \bar{g} = \sum_{i=1}^{21} \phi_i$$

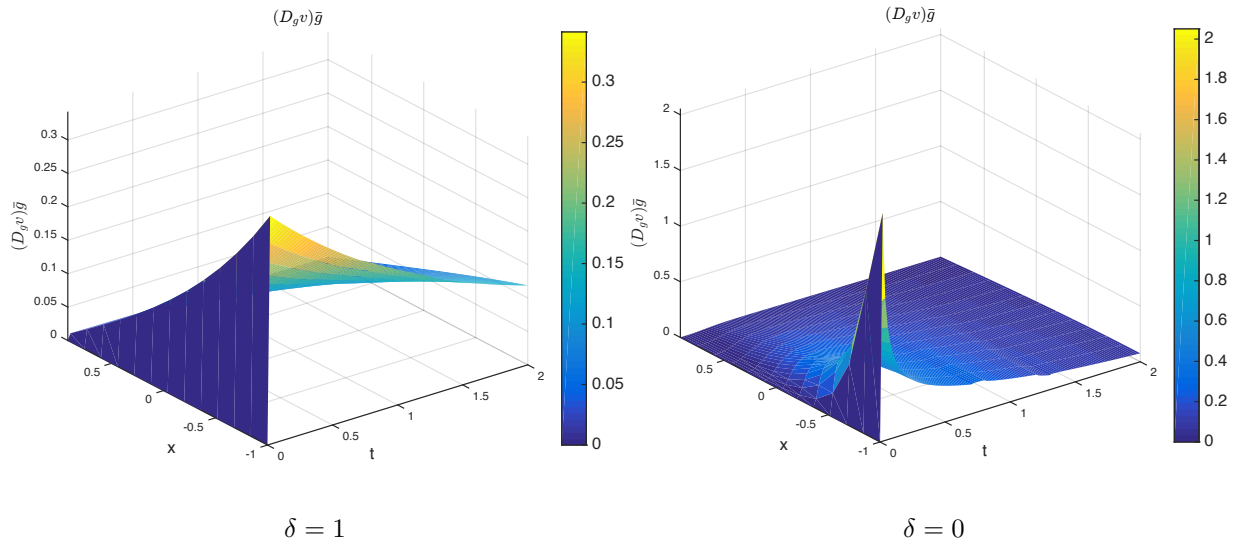


Figure 22: Sensitivity functions of discharge velocity (v) with respect to boundary stress $g_5 = \mathcal{G}_q, q = \infty$ in the direction of $\bar{\psi} = \sum_{i=1}^{21} \phi_i$ when $\delta = 1$ (left) and $\delta = 0$ (right).

Observations: From Figures 17-19 we can see again that the magnitude of the sensitivities is bigger when $\delta = 0$ than when $\delta = 1$. This suggests that the purely elastic model is more sensitive to the boundary data than the visco-elastic model. We also note that in the elastic case $\delta = 0$, the effect of the boundary data on the solutions (u, p) is quite significant throughout the domain. In comparison, the boundary effects on (u, p) diminish as we go farther from the boundary for the case when $\delta = 1$.

We also observe that the sensitivity graphs appear to be similar to those obtained in Case 3, where the permeability was constant. Here, even though the permeability is nonlinear, the system is driven only by the boundary stress datum g_5 . In comparison, the sensitivities obtained in the previous case (Case 4) are quite different, and this could be explained by the system's complexity due to the interaction between the nonlinear permeability k , and non-zero body force F and net volumetric fluid production rate S .

5.6 Boundary sensitivity as a function of viscosity parameter δ

In all of the previous examples, we can see that states (u, p, v) are more sensitive to the boundary data in the purely elastic case $\delta = 0$ in comparison to the visco-elastic scenario $\delta = 1$. In this section, we further investigate the importance of the viscosity parameter by considering a variety of values for δ , and studying the effect of the boundary stress g on the solid displacement, fluid pressure, and discharge velocity in all these cases. Based on the analysis provided in [12], we focus on two main ranges for δ : $0 \leq \delta \leq 1$ vs. $1 \leq \delta \leq 2$. In these computations, we use the same set up as in Case 4, with constant boundary function $g_4 = 1$.

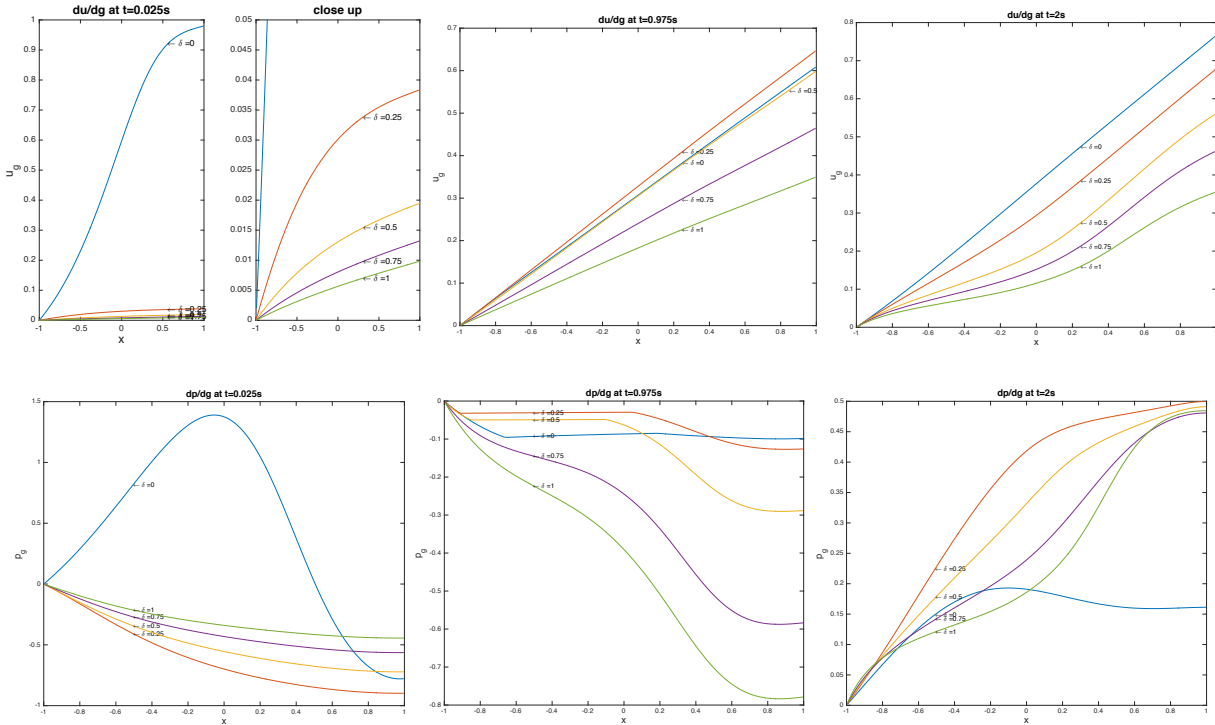


Figure 23: Sensitivity of u and p to boundary stress for various values of $0 \leq \delta \leq 1$

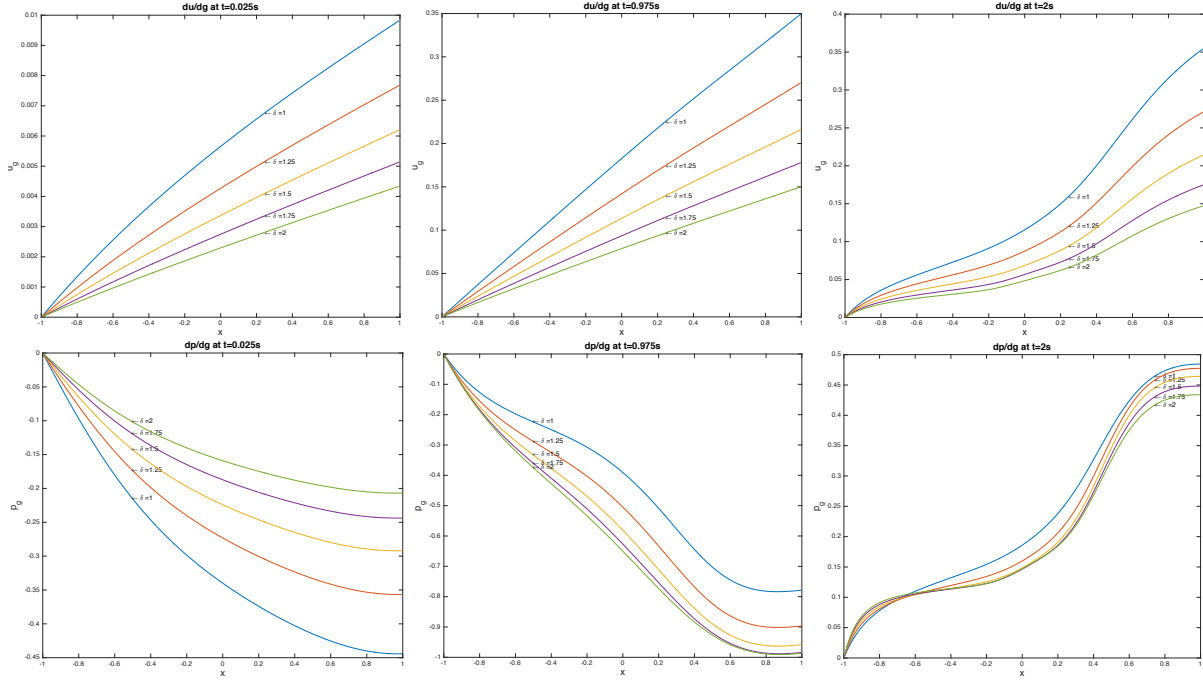


Figure 24: Sensitivity of u and p to boundary stress for various values of $1 \leq \delta \leq 2$

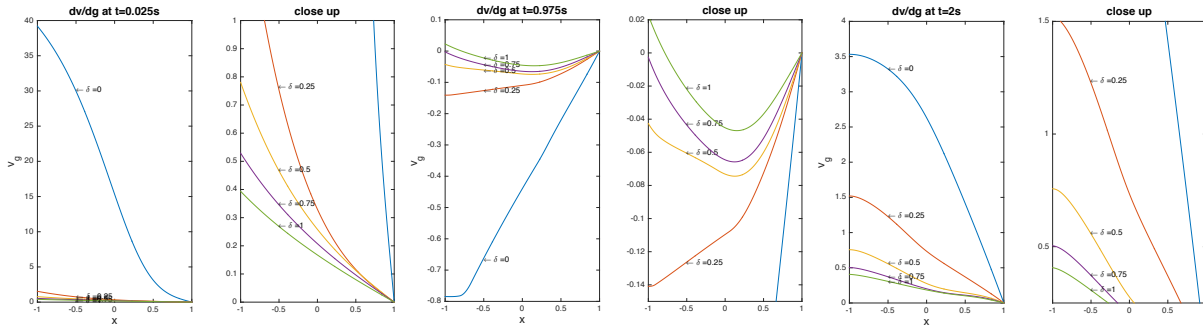


Figure 25: Sensitivity of v to boundary stress for various values of $0 \leq \delta \leq 1$

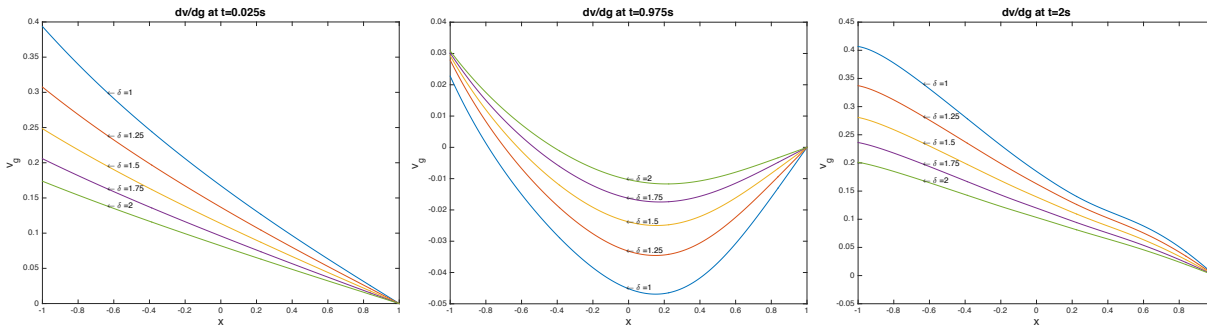


Figure 26: Sensitivity of v to boundary stress for various values of $1 \leq \delta \leq 2$

First we discuss the behaviors of the sensitivities of the elastic displacement with respect to the boundary datum g , shown in Figures 23 and 24 .

For $0 \leq \delta \leq 1$, we can see that the sensitivities of the elastic displacement w.r.t g do not follow a “prescribed” pattern, as we have 2 different scenarios at the three times chosen. At times $t = 0.025$ and $t = 2$, we note that the solution is much more sensitive for $\delta = 0$ and there is clear pattern: the more visco-elasticity, i.e., the bigger the δ , the elastic displacement is less sensitive to g . At time $t = .975$, the elastic sensitivity is two to three times smaller for values of δ close to 1 compare to values of δ close to 0. However, it can also be observed that the sensitivity for $\delta = .25$ is slightly bigger than the one computed for $\delta = 0$ through the space domain. This could suggest that there is a range of small values of δ around 0 for which the sensitivity of the elastic solution stays within the same range as the one in the case of $\delta = 0$.

In comparison, for $1 \leq \delta \leq 2$, the graphs for the elastic sensitivities show a solid trend for all the times considered: the larger the value of δ , the smaller the sensitivity. This suggests that, for the particular case at hand, the value $\delta = 1$ is a “safe value” in terms of assuring that the elastic sensitivity will continue to decrease as δ increases above 1.

Comparing Figures 23 and 24, we note that the magnitudes of the sensitivities are smaller for $1 \leq \delta \leq 2$ compared to $0 \leq \delta \leq 1$, which agrees with what we observed in the previous investigations (Case 1 - Case 5).

Regarding the sensitivities of the pressure with respect to the boundary datum g , when $0 \leq \delta \leq 1$, the behavior of the sensitivities is “complex”. The various curves are intersecting with each other, hinting that different parts of the domain would have a different sensitivity to the data depending on the level of viscoelasticity. Thus, the choice of δ would affect differently various regions within the domain. Even in the case of $1 \leq \delta \leq 2$, the graphs do not show any pattern: at $t = 0.025$, the sensitivity decreases as δ gets larger, at $t = 0.975$, the behavior is quite the opposite, with the sensitivity increasing as δ gets larger, and at $t = 2$ the graphs of the sensitivities intersect and reverse their order in magnitude at around $x = -.65$.

The sensitivities of the discharge velocity with respect to the boundary datum g show a clear “order” in magnitudes in most of the cases considered (see Figures 25 and 26. For both $0 \leq \delta \leq 1$ and $1 \leq \delta \leq 2$, the sensitivity increases as δ gets smaller. There is one exception at time $t = .975$, in the case of $1 \leq \delta \leq 2$: the boundary source g is applied at $x = 1$, and around in the interval $x \in [-1, -.4]$, the sensitivities lose the expected “ordering”, as their magnitudes fluctuate close to 0.

It is also interesting to see the big difference in the magnitudes of the sensitivities between $\delta = 0$ and values of δ close to 2. This again suggests that the discharge velocity becomes heavily sensitive to the boundary data of traction when visco-elasticity is not present in the system.

6 Conclusions and Relevance

All our numerical results show that the solution (u, p, v) is more sensitive to boundary traction in the elastic case than in the visco-elastic scenario. This could explain why in the theoretical results provided in [12], the boundary source was required to have higher time regularity in order to obtain solution (u, p) in L^2 in space and time, and with appropriate energy estimate in terms of data, in the purely elastic case.

The effects of the boundary source are most significant for the discharge velocity v , especially in the $\delta = 0$ case. This is very important, as the numerical investigation in [12] hinted that the fluid energy (which is dependent on the discharge velocity) becomes unbounded as the boundary source of traction loses H^1 -smoothness in time, and visco-elasticity is no longer present.

The results of this sensitivity study also offers valuable insights on the potential mechanisms that could be leveraged to control fluid flow in deformable porous media in specific applications. In [6] we also looked at the sensitivity of the solution with respect to the boundary source ψ . Interestingly, the fluid-dynamical variables v and p appear to be more sensitive to changes in g than to changes in ψ . This suggests that, in order to control fluid velocity and pressure, it would be much more effective to act on the boundary conditions for the solid structure, namely the traction g , rather than on the boundary conditions for the velocity itself, namely ψ . The solid displacement u appears to be the least sensitive to changes in g and ψ ; this motivates one to look for other ways to control the solid displacement, such as by acting on the material elastic and viscoelastic properties. In addition, this finding also shows that small changes in the solid displacement may actually correspond to big changes in fluid velocity and pressure, thereby suggesting that monitoring the sole solid displacement might not be indicative of the fluid-dynamical state inside the medium.

Another important observation is that the areas within the domain exhibiting highest sensitivity to data differ from case to case, depending on whether volumetric sources of mass and momentum are present and on whether the permeability depends on dilation. This finding suggests that each case should be studied in detail, should the control problem be of interest in a specific application under particular conditions. A similar remark should be made for the influence of the viscoelastic parameter δ . Even though, in general, lower sensitivities are associated with higher values of δ , the results reported in Section 5.6 exhibit a complex behavior in space and time depending on the range of δ . This might be due to the fact that viscoelasticity introduces a time delay between stress and strain within the material, thereby strongly affecting the dynamic behavior of the system in time and space. Depending on the length of the observational time and the elastic and viscoelastic properties of the material, the specific ranges for δ ensuring a monotonic trend in the sensitivity parameters may vary. To further understand this issue, we believe that it would be useful to perform the sensitivity analysis on a dimensionless version of the problem, where relevant physical and geometrical parameters of the problem are combined in dimensionless numbers that can be used to establish some equivalences between behaviors of apparently different systems. This is currently work in progress.

Acknowledgments

This research was supported in part by the Air Force Office of Scientific Research under grant numbers AFOSR FA9550-12-1-0188 and AFOSR FA9550-15-1-0298, and in part by the National Science Foundation under grant NSF CAREER DMS-1555062.

We would like to express our thanks to Kristen Tillman for her contribution in the early stage of this project.

References

- [1] W. Kyle Anderson and Eric J. Nielsen, *Sensitivity analysis for Navier-Stokes equations on unstructured meshes using complex variables*, AIAA Journal, **39** (2001).
- [2] W. Kyle Anderson, Eric J. Nielsen, and D.L. Whitfield, *Multidisciplinary sensitivity derivatives using complex variables*, Technical report, Engineering Research Center Report, Mississippi State University, mSSU-COE-ERC-98-08, July, 1998.
- [3] R. P. Araujo and D. L. Sean McElwain. A mixture theory for the genesis of residual stresses in growing tissues I: a general formulation. *SIAM J. Appl. Math.*, 65(4):1261–1284, 2005.
- [4] H.T. Banks, K. Bekele-Maxwell, L. Bociu, M. Noorman and K. Tillman, *The complex-step method for sensitivity analysis of non-smooth problems arising in biology*, Eurasian Journal of Mathematical and Computer Applications **3** (2015), 15-68.
- [5] H.T. Banks, K. Bekele-Maxwell, L. Bociu, C. Wang, *Sensitivity via the complex-step method for delay differential equations with non-smooth initial data*, CRSC-TR16-09, Center for Research in Scientific Computation, N. C. State University, Raleigh, NC, July, 2016, Quarterly of Applied Mathematics November 2, 2016. <http://dx.doi.org/10.1090/qam/1458>.
- [6] H.T. Banks, K. Bekele-Maxwell, L. Bociu, M. Noorman, and G. Guidoboni, *Sensitivity analysis in poro-elastic and poro-visco-elastic models*, CRSC-TR17-01, Center for Research in Scientific Computation, N. C. State University, Raleigh, NC, February 2017,
- [7] H.T. Banks, S. Dediu, and S.E. Ernstberger, *Sensitivity functions and their uses in inverse problem*, J. Inverse and Ill-posed Problems, **15** (2006), 683 - 708.
- [8] H.T. Banks, S. Hu, and W.C. Thompson, *Modeling and Inverse Problems in the Presence of Uncertainty*, Chapman & Hall/CRC Press, Boca Raton, FL, 2014.
- [9] H.T. Banks and H.T. Tran, *Mathematical and Experimental Modeling of Physical and Biological Processes*, CRC Press, Boca Raton, FL, July, 2008, 308pp., 2009.
- [10] G.A. Behie, A. Settari, and D.A. Walters, *Use of coupled reservoir and geomechanical modeling for integrated reservoir analysis and management*, Technical Report, Canadian International Petroleum Conference, Calgary, Canada, 2000.
- [11] M.A. Biot, *General theory of three-dimensional consolidation*, J. Appl. Phys., 12(2) (1941), 155-164.
- [12] L. Bociu, G. Guidoboni, R. Sacco, and J. Webster, *Analysis of nonlinear poro-elastic and poro-viscoelastic models*, Archive for Rational Mechanics and Analysis, **222**, (2016) 1445-1519.
- [13] Jeff Borggaard, Vitor Leite Nunes *Fréchet sensitivity analysis for partial differential equations with distributed parameters*, Proceedings of the 2011 American Control Conference. IEEE, 2011.
- [14] M.S. Bruno, *Geomechanical analysis and decision analysis for mitigating compaction related casing damage*, Society of Petroleum Engineers, 2001.

- [15] Y. Cao, S. Chen, and A.J. Meir, *Analysis and numerical approximations of equations of nonlinear poroelasticity*, *DCDS-B*, 18 (2013), 1253-1273.
- [16] Y. Cao, S. Chen, and A.J. Meir, *Quasilinear Poroelasticity: Analysis and Hybrid Finite Element Approximation*, *Num. Meth. PDE*, published online (2014) DOI: 10.1002/num.21940.
- [17] P. Causin, G. Guidoboni, A. Harris, D. Prada, R. Sacco, and S. Terragni, *A poroelastic model for the perfusion of the lamina cribrosa in the optic nerve head*, *Mathematical Biosciences*, 257 (2014), 33-41.
- [18] D. Chapelle, J. Sainte-Marie, J.-F. Gerbeau, I. Vignon-Clementel, *A poroelastic model valid in large strains with applications to perfusion in cardiac modeling*, *Comput. Mech.*, 46(1) (2010), 91-101.
- [19] O. Coussy, *Poromechanics*, Wiley, 2004.
- [20] S.C. Cowin, *Bone poroelasticity*, *J. Biomech.*, 32(3) (1999), 217-238.
- [21] E. Detournay and A.H.-D. Cheng, *Fundamentals of poroelasticity, Chapter 5 in Comprehensive Rock Engineering: Principles, Practice and Projects, Vol. II, Analysis and Design Method*, ed. C. Fairhurst, Pergamon Press, (1993), 113-171.
- [22] E. Detournay and A.H.-D. Cheng, *Poroelastic response of a borehole in non- hydrostatic stress field*, *International Journal of Rock Mechanics and Mining Sciences*, 25, 1988, 171-182.
- [23] M.B. Dusseault, M.S. Bruno, and J. Barrera, *Casing shear: Causes, cases, cures*, Society of Petroleum Engineers, 2001.
- [24] A. J. H. Frijns. *A four-component mixture theory applied to cartilaginous tissues: Numerical modelling and experiments*. Thesis (Dr.ir.)—Technische Universiteit Eindhoven (The Netherlands) 2000.
- [25] D. Garagash and E. Detournay, *An analysis of the influence of the pressurization rate on the borehole breakdown pressure*, *Journal of Solids and Structures*, 1997.
- [26] G. Guidoboni, A. Harris, L. Carichino, Y. Arieli, and B. A. Siesky, *Effect of intraocular pressure on the hemodynamics of the central retinal artery: a mathematical model*, *Mathematical Biosciences and Engineering*, 11.3, 2014, 523-546.
- [27] C.T. Hsu and P. Cheng, *Thermal dispersion in a porous medium*, *Int. J. Heat Mass Tran.*, 33 (8) (1990), pp. 1587 - 1597.
- [28] J. Hudson, O. Stephansson, J. Andersson, C.-F. Tsang, and L. Ling, *Coupled T-H-M issues related to radioactive waste repository design and performance*, *International Journal of Rock Mechanics and Mining Sciences*, 38:143-161, 2001.
- [29] J.M. Huyghe, T. Arts, D.H. van Campen and R.S. Reneman, *Porous medium finite element model of the beating left ventricle*, *Am. J. Physiol.*, 262 (1992), 1256-1267.
- [30] J.-M. Kim and R. Parizek, *Numerical simulation of the Noordbergum effect resulting from groundwater pumping in a layered aquifer system*, *Journal of Hydrology*, 202:231-243, 1997.
- [31] S. M. Klisch. *Internally constrained mixtures of elastic continua*, *Math. Mech. Solids*, 4:481-498, 1999.

- [32] W.M. Lai, J.S. Hou and V.C. Mow, *A triphasic theory for the swelling and deformation behaviors of articular cartilage*, ASME J. Biomech. Eng., 113 (1991), 245-258.
- [33] Terri Langford, *Northwest Houston sinking faster than coastal areas*, Reporter-News.com, Aug. 28 1997.
- [34] G. Lemon, J. R. King, H. M. Byrne, O. E. Jensen, and K. M. Shakesheff. *Mathematical modelling of engineered tissue growth using a multiphase porous flow mixture theory*, J. Math. Biol., 52:571–594, 2006.
- [35] N. Lubick, *Modeling complex, multiphase porous media systems*, SIAM News, 5(3), 2002.
- [36] J. N. Lyness, *Numerical algorithms based on the theory of complex variables*, Proc. ACM 22nd Nat. Conf., 4 (1967), 124 - 134.
- [37] J. N. Lyness and C. B. Moler, *Numerical differation of analytic functions*, SIAM J. Numer. Anal., 4 (1967), 202 - 210.
- [38] Joaquim R. R. A. Martins, Ilan M. Kroo, and Juan J. Alonso. *An automated method for sensitivity analysis using complex variables*, AIAA Paper 2000-0689 (Jan.), 2000.
- [39] Joaquim R. R. A. Martins, Peter Sturdza, and Juan J. Alonso. *The complex-step derivative approximation*, Journal ACM Transactions on Mathematical Software (TOMS), 2003.
- [40] Misra S, Macura KJ, Ramesh KT, Okamura AM, *The Importance of Organ Geometry and Boundary Constraints for Planning of Medical Interventions*, Medical engineering and physics. 2009;31(2):195-206. doi:10.1016/j.medengphy.2008.08.002.
- [41] V.C. Mow, S.C. Kuei, W.M. Lai and C.G. Armstrong, *Biphasic creep and stress relaxation of articular cartilage in compression: theory and experiments*, ASME J. Biomech. Eng., 102 (1980), 73-84.
- [42] S. Owczarek, *A Galerkin method for Biot consolidation model*, Math. Mech. Solids, 15 (2010), 42-56.
- [43] P. J. Phillips and M. F. Wheeler, *A coupling of mixed and continuous Galerkin finite-element methods for poroelasticity I: the continuous in time case*, Computational Geosciences 11.2 (2007): 131-144.
- [44] P.J.Phillips and M.F.Wheeler, *A coupling of mixed and continuous Galerkin finite-element methods for poroelasticity II: the continuous in time case*, Computational Geosciences 11.2 (2007): 145-158.
- [45] P.J.Phillips and M.F.Wheeler, *A coupling of mixed and continuous Galerkin finite-element methods for poroelasticity* , Computational Geosciences 12.4 (2008): 417-435.
- [46] L. Preziosi and A. Tosin. *Multiphase modelling of tumour growth and extracellular matrix interaction: mathematical tools and applications*, J. Math. Biol., 58:625–656, 2009.
- [47] R. Rajapakse, *Stress analysis of borehole in poroelastic medium*, Journal of Engineering Mechanics, 119(6):1205 - 1227, 1993.
- [48] T. Roose, P.A. Netti, L. Munn, Y. Boucher, and R. Jain, *Solid stress generated by spheroid growth estimated using a linear poroelastic model*, Microvascular Research, 66:204–212, 2003.

- [49] J. Rutqvist and C.-F. Tsang, *Analysis of thermal-hydrologic-mechanical behavior near an emplacement drift at Yucca mountain*, Journal of Contaminant Hydrology, 62-63:637-652, 2003.
- [50] A. Settari and D.A. Walters, *Advances in coupled geomechanical and reservoir modeling with applications to reservoir compaction*, Technical Report, SPE Reservoir Simulation Symposium, Houston, TX, 1999.
- [51] R.E. Showalter, *Diffusion in poro-elastic media*, JMAA, 251 (2000), pp. 310–340.
- [52] A. Smillie, I. Sobey, and Z. Molnar, *A hydro-elastic model of hydrocephalus*, Technical report, Oxford University Computing Laboratory: Numerical Analysis Group, 2004.
- [53] W. Squire and G. Trapp, *Using complex variables to estimate derivatives of real functions*, SIAM Review, **10** (1998), 100 - 112.
- [54] N. Su and R.E. Showalter, *Partially saturated flow in a poroelastic medium*, DCDS-B, 1 (2001), 403–420.
- [55] Sun W, Sacks MS, Scott MJ, *Effects of Boundary Conditions on the Estimation of the Planar Biaxial Mechanical Properties of Soft Tissues*, ASME. J Biomech Eng. 2005;127(4):709-715. doi:10.1115/1.1933931.
- [56] C.C. Swan, R.S. Lakes, R.A. Brand, and K.J. Stewart, *Micromechanically based poroelastic modeling of fluid flow in haversian bone*, Journal of Biomechanical Engineering, 125(1):25-37, Feb. 2003.
- [57] K. Terzaghi, *Principle of soil mechanics*, Eng. News Record, A Series of Articles, 1925.
- [58] Michael D Vahey, Daniel A Fletcher, *The biology of boundary conditions: cellular reconstitution in one, two, and three dimensions*, Current Opinion in Cell Biology, Volume 26, February 2014, Pages 60-68, ISSN 0955-0674, <http://dx.doi.org/10.1016/j.ceb.2013.10.001>. (<http://www.sciencedirect.com/science/article/pii/S0955067413001543>)
- [59] Stephen D. Waldman, Michael Lee, *Boundary conditions during biaxial testing of planar connective tissues. Part 1: Dynamic Behavior*, J. Mater. Sci. Mater. Med. 13.10 (Oct 2002), 933-938.
- [60] H. F. Wang, *Theory of Linear Poroelasticity with Applications to Geomechanics and Hydrogeology*, Princeton University Press, Princeton, N.J., 2000.
- [61] Y. Wang and M. Dusseault, *A coupled conductive-convective thermo-poroelastic solution and implications for wellbore stability*, Journal of Petroleum Science and Engineering, **38** (2003)187-198.
- [62] A. Zenisek, *The existence and uniqueness theorem in Biot's consolidation theory*, Appl. Math., 29 (1984), 194-211.